NASA Technical Memorandum 86348

Comparison of Wind Velocity in Thunderstorms Determined From Measurements by a Ground-Based Doppler Radar and an F-106B Airplane

J. W. Usry, R. Earl Dunham, Jr.,
and J. T. Lee

APRIL 1985

NASA

NASA Technical Memorandum 86348

Comparison of Wind Velocity in Thunderstorms Determined From Measurements by a Ground-Based Doppler Radar and an F-106B Airplane

J. W. Usry and R. Earl Dunham, Jr.
Langley Research Center
Hampton, Virginia

J. T. Lee
National Severe Storms Laboratory
National Oceanic and Atmospheric Administration
Norman, Oklahoma

National Aeronautics
and Space Administration

**Scientific and Technical
Information Branch**

1985

Summary

The NASA Storm Hazards Program was initiated to improve the knowledge and understanding of atmospheric processes and their effects on aircraft flight operations in the vicinity of storms. An instrumented F-106B airplane was used to penetrate thunderstorms and to make measurements of the wind at points along the flight path. During these flights, a ground-based Doppler radar also made independent measurements of the wind. This report presents the results of five airplane penetrations of two storms in 1980 and six penetrations of one storm in 1981. Comparisons were made between the wind velocity measured by the radar and the airplane. Least-squares regression lines were calculated, and correlation coefficients of 0.88 and 0.78 were obtained for the 1980 data and part of the 1981 data, respectively. This combined data set also had a correlation coefficient of 0.88. Although the correlations may be as good as can be expected for comparisons of this type, it is suggested that improvements in the experimental technique could possibly improve the results.

Introduction

The Storm Hazards Program was initiated to improve the knowledge and understanding of atmospheric processes and their effects on aircraft flight operations in the vicinity of severe storms. Results from the program will be useful in improving the design of aircraft and systems for storm hazards protection and for the detection and avoidance of hazardous weather conditions (ref. 1). Since its inception, the primary emphasis of the program has been on characterizing lightning and its effects on advanced aircraft avionics and composite structures (refs. 2 and 3). In the initial phase of the program, an instrumented NASA twin-engine light transport airplane flew around the periphery of storms to detect and locate lightning discharges. Later, thunderstorm penetrations were made in an F-106B airplane instrumented to make extensive measurements of the thunderstorm environment. These measurements included the three wind components at points along the flight path. Also during these flights, a ground-based Doppler radar made independent measurements of the wind velocity along the radar beam. Interest in using a Doppler radar for characterizing the wind velocity in the vicinity of thunderstorms has increased recently because of its potential application for improving aviation safety. For this reason, these two independent measurements of the wind velocity in thunderstorms were compared. The purpose of this paper is to present the results of those comparisons.

Flight operations in 1980 and 1981 were conducted in Norman, Oklahoma, in a cooperative effort with the National Severe Storms Laboratory (NSSL). Generally, the method of operation was to locate a storm by means of ground-based radars, deploy the NASA F-106B airplane, direct the airplane to the vicinity of the storm, and fly through the storm several times before returning to the base. No attempt was made, however, to achieve simultaneous or coextensive velocity measurements by the airplane and ground-based Doppler radar. Flight operations included five thunderstorm penetrations in June 1980 and six penetrations in April 1981. Radial velocity contours measured by Doppler radar are presented for each thunderstorm penetration with the F-106B ground track superimposed on the contours. Comparison plots of the airplane and radar radial velocity data are presented for 1980, 1981, and the combined data for both years.

Symbols and Abbreviations

A_z	vertical acceleration, positive up, g units
AIS	aircraft instrument system
a	unit vector from airplane to radar
g	acceleration due to gravity, 9.807 m/s^2
h_p	altitude determined from pressure measurement (pressure altitude), m
INS	inertial navigation system
l	distance between INS package and flow vanes along longitudinal axis of F-106B, m
NSSL	National Severe Storms Laboratory
p	roll velocity of F-106B about body x-axis, rad/s
q	pitch velocity of F-106B about body y-axis, rad/s
q'_c	measured dynamic pressure
r	yaw velocity of F-106B about body z-axis, rad/s
T	integration interval, s
t	time, s
$\mathbf{V}$	velocity of F-106B relative to air mass, m/s
$\mathbf{V}_I$	inertial velocity of F-106B, m/s
$V_{x'}, V_{y'}, V_{z'}$	components of $\mathbf{V}_I$, m/s

$(V_{z'})_0$	initial value of inertial velocity used in equation (A6), m/s
$\mathbf{W}$	wind velocity, m/s
W_r	radial wind velocity, m/s
W_{ra}	radial wind velocity computed from F-106B data, m/s
W_{rr}	radial wind velocity computed from Doppler radar data, m/s
$W_{x'}, W_{y'}, W_{z'}$	components of $\mathbf{W}$ in inertial axis system, positive north, east, and down, m/s
x, y, z	body axes of F-106B, dimensionless
x', y', z'	inertial axes, dimensionless
α	angle of attack as measured by flow vanes and corrected for flow-field effects, deg
α_m	angle of attack as measured by flow vanes, deg
β	angle of sideslip as measured by flow vanes (no flow-field corrections used), deg
Γ	transformation matrix defined by equation (A3) of appendix
Δp_s	difference between measured static pressure and free-stream static pressure
θ, ϕ, ψ	Euler angles, deg

Experimental Apparatus

The experimental apparatus used in the Storm Hazards Program at the NSSL is described in detail in references 1–5. For that reason, only the equipment and systems pertinent to data presented herein are described in this paper.

Research Airplane and Systems

A photograph of the NASA F-106B airplane is shown in figure 1. The airplane is an all-weather, two-seat, delta-wing interceptor with a leading-edge sweep of 60°. Modifications were made to the airplane especially for the Storm Hazards Program and were described in reference 3. Basic characteristics of the airplane (from ref. 2) are listed in table I. The airplane was equipped with an X-band color weather radar to display precipitation reflectivity contours, an aircraft instrument system (AIS), and an inertial navigation system (INS).

The aircraft instrument system measurements included angles of attack and sideslip, airplane body rates, pitot-static and dynamic pressures, total temperature, airplane center-of-gravity accelerations, and lateral and longitudinal stick position. A 14-track magnetic tape recorder and time code generator were used for recording time histories of the various measurements. The AIS also recorded the output of the INS. Data were recorded at a rate of 20 samples per second.

The INS was designed for commercial use to provide aircraft navigation. The INS measurements included latitude and longitude; pitch, roll, and true heading; vertical acceleration; and horizontal components of airplane ground speed. Experience with this system as used on the F-106B missions indicates a typical position error of about 1 nautical mile per hour of flight.

A list of the parameters recorded by the AIS and used to derive the three components of wind are presented in table II. Also listed are the instrument range, frequency response, 1σ error, and measurement resolution. The dynamic-pressure sensor and flow vanes were located on the nose boom. Rate gyros were located in the internal weapons bay. The INS and the longitudinal, lateral, and normal accelerometers were mounted at the center of gravity of the airplane. The vertical accelerometer was an integral part of the INS platform. Pitot-static pressure and air total temperature probes were located beneath the nose of the airplane.

Doppler Radar

The NSSL has a matched pair of Doppler radars, one located at Norman and the other at Cimarron, for scanning thunderstorms. During the Storm Hazards Program, no storms entered the coverage area common to both radars, and for that reason, all Doppler radar data were obtained by the radar located at Norman.

Doppler radar characteristics for the radar located at Norman are listed in table III. (See ref. 6.) The radar had a half-power beam width of 0.8°, a wavelength of 10.5 cm, and a peak power of 750 kW. The pulse width was 1 μs, and a scan rate of 6 deg/s was used. The pulse repetition time was normally 768 μs, and 64 samples were used to estimate the mean velocity. The dwell time was typically 50 ms. After completing an azimuthal scan, the elevation was stepped and the scan was repeated. A scan at each of three elevation angles was made, and data at three altitudes were obtained such that the interval between the low and high altitudes included the altitude at which the F-106B was flying.

The volume in space sampled by the radar (radar resolution volume) for a zero antenna scan rate has dimensions defined by the pulse width (depth of volume), antenna beam width, and the range from the radar to the sample volume. (Beam width and range define the cross-sectional area perpendicular to the centerline of the beam.) The resolution volume is an inherent characteristic of the radar and is smaller than the actual volume sampled in space. The reason for this is that the Doppler spectrum is determined from many transmitted pulses, and as the radar scans, the volume contributing to the spectrum is larger than the resolution volume. This larger volume is defined to be the measurement volume (ref. 7). The measurement and resolution volumes were assumed to be equal for these experiments.

Analysis Method

F-106B Measurements

The wind radial velocity along the Doppler radar beam from the F-106B to the radar was derived from measurements of the parameters listed in table II. The wind vector was determined by the method presented in the appendix. The wind velocity data as determined from the F-106B measurements were computed at a rate of 20 samples per second. Since the Doppler radar radial velocity was actually an average over the radar measurement volume, the airplane data were averaged over a 5-s interval in order to make the comparisons between the radar and airplane data. This interval was the time required for the F-106B to travel about 1 km, which is the diameter of a sphere with a volume equivalent to the radar measurement volume at the nominal radar range (140 km) of the tests. The sensitivity of the airplane radial velocity measurements to averaging intervals of 2, 5, and 10 s is shown in figure 2. As would be expected, larger averaging intervals smooth the data by removing variations in the radial velocity due to turbulence and sharp-edged updraft or downdraft regions.

Doppler Radar

Doppler radar measures target speeds of precipitation particles as the beam sweeps the thunderstorm. Motion of the particles toward or away from the radar (radial velocity) is deduced from minute shifts in the microwave frequency of precipitation echoes. Because the volume sampled in space by the radar contains many targets, the radar actually measures a spectrum of radial velocities. The first moment of the Doppler spectrum is the mean radial velocity of the particles in the volume sampled. Principles of pulsed Doppler radar may be found in references 8 and 9. Some details on Doppler radar data reduction procedures may be found in reference 1.

Doppler radar radial velocity contours on constant altitude surfaces as a function of position from the Doppler radar as shown in figure 3 were provided by the NSSL. The contours were produced from sector-scans of the storm that were made during the time that the F-106B was flying through the storm. Generally the radar data measurements required about 3 min and were synchronized with the time of the F-106B measurements within 2 min. Velocity contours for the 1980 data were provided by the NSSL at the altitude flown by the F-106B. Velocity contours for the 1981 data, however, were provided at three altitudes, and it was necessary to interpolate to the F-106B altitude. The interpolation method used is illustrated in figure 3.

Velocity contours at three altitudes are shown in figure 3(a). It was assumed that the wind fields were frozen during the time required for the F-106B to traverse the thunderstorm. There are several possible approaches for comparing the Doppler frozen wind field data, which were measured as a function of position, with the airplane data, which were measured as a function of time along the flight path. One possible approach, for example, would be to superimpose the velocities measured by the airplane at positions on the frozen wind fields. A second approach would be to take the Doppler radar contour data at a given position and transform it to an effective time history along the flight path. The latter approach was chosen to make these comparisons. For this method a radial velocity effective time history was constructed at each altitude to represent the Doppler radar radial velocity at points along the F-106B flight path. This was done by calculating the F-106B ground track as a function of position from the Doppler radar and plotting the track over the contours at each altitude. Elapsed time along the flight path is indicated in figure 3(a). The radial velocity values as a function of position were extracted at each altitude and plotted in figure 3(b) as a function of elapsed time along the flight path. For the penetration shown, the F-106B altitude was 3.7 km. Values of the radial velocity at that altitude were determined by interpolation and are also shown in figure 3(b). Direction of flight through the storm and direction to the Doppler radar at Norman from the F-106B are also indicated in figure 3(a).

Results and Discussion

Radial velocity data derived from Doppler radar and F-106B measurements for flights made in June

1980 are shown in figures 4–8. Figures 4 and 5 show results for two passes through the thunderstorm at an altitude of 4.6 km on June 16. Figures 6–8 show results for three passes through another thunderstorm at an altitude of 4.9 km on June 17. The average distance from the radar to the F-106B for the data shown in figure 4 was 113 km, and for the data shown in figure 7, the average distance was 155 km. Average distances for the other penetrations fell within those boundaries.

Ground tracks derived from the F-106B INS data are shown in the (a) parts of figures 4–8 superimposed on the Doppler radar radial velocity contour plots. The direction of flight of the F-106B airplane through the storm is indicated on each figure as well as the direction toward the Doppler radar at Norman.

The (b) parts of figures 4–8 show time histories of the radial velocity derived from the F-106B measurements (see eqs. (A2) and (A4) in the appendix) and from the Doppler radar data presented in the (a) parts of figures 4–8. These data were used to make the comparison plot shown in figure 9. The regression line in figure 9 was derived from 96 data points obtained by reading the radial velocity values at 15-s intervals along the ground tracks in figures 4–8 and matching these points in time with the F-106B values. The correlation coefficient was 0.88.

Figures 10–15 show the radial velocity contour plots and time histories for a flight conducted on April 22, 1981. The F-106B made six passes through the thunderstorm: two passes at an altitude of 3.7 km, one pass at 4.6 km, two passes at 6.1 km, and one pass at 6.0 km. Contour plots at the altitude nearest the F-106B altitude are shown in figures 10–15. These altitudes were within 400 m of the F-106B altitude for the data in figures 10–14, and within 300 m for the data in figure 15. The range from the radar to the F-106B generally was greater than 120 km. Figure 16 shows a comparison plot of the 1981 radial velocity data derived from figures 10–15. The regression line was derived from 93 data points, and the correlation coefficient was 0.47.

Comparisons of the 1980 Doppler radar and airplane radial velocity data summarized in figure 9 were considerably better (Correlation coefficient = 0.88) than the 1981 data summarized in figure 16 (Correlation coefficient = 0.47). It is reasonable to expect that the correlation coefficients would be comparable. For example, the 1980 data were derived from two flights (five passes) through two thunderstorms, and the 1981 data were derived from one flight (six passes) through one thunderstorm. Methods used to derive the Doppler radar radial velocity time histories along the F-106B flight path for both data sets were essentially the same. Also, both regression lines were calculated from about 100 data points.

Apparently the correlation coefficient in figure 16 was lower than the correlation coefficient in figure 9 because of significant differences in the F-106B and Doppler radar radial velocity values for three of the six passes (i.e., passes 3, 4, and 6) through the thunderstorm in April 1981. These differences were shown in figures 12(b), 13(b), and 15(b). It is possible that the differences were caused by large variations in the wind field within the radar measurement volume. For example, the radar measurements were averages over the measurement volume, whereas the F-106B measurements were along the flight path (a line) in a horizontal plane in the measurement volume. The average distance of the F-106B from the Doppler radar for each of the three passes was about 140 km. This means that the cross section of the radar measurement volume perpendicular to the beam had a diameter of about 2 km, and the radar would have averaged the wind field with that cross section. It is also possible that the radar-derived altitudes for the contour plots could at times have been in error at these long ranges because of refractivity variations along the propagation path. In all cases, the radar data were subjected only to a standard earth curvature refractivity correction.

Figures 17(a)–17(c) show the F-106B radial velocity time histories for penetrations 3, 4, and 6 derived by interpolating between three altitudes. These figures show that the time histories above and below the F-106B altitude were similar, and radial velocity magnitudes were not significantly different, except for the first half of penetration 4 in figure 17(b) and the latter part of penetration 6 in figure 17(c). To make these interpolations, it was assumed that the airplane flew through the storm at a constant altitude that was equivalent to the altitude at entry to the storm. Actually the altitude within the storm may have changed because of sudden changes in the wind field. Experience has shown that these changes rarely exceed 200 m during a penetration but may have occasionally been 300 m (approximately 1 time per 100 penetrations). Also the altitude at entry was based on barometric pressure and may have been different from the geometric altitude representing the radar data at that altitude. These uncertainties along with probable time differences between the airplane and radar measurements, which could mean that the storm dynamics at a given altitude had changed, may account for the trends shown in figures 17(b) and 17(c) and for the differences seen in figures 13(b) and 15(b). These trends (see figs. 17(b) and 17(c)) suggest that the differences in the wind

field as a function of altitude may account for the smaller correlation coefficient for the 1981 data in figure 16. In fact, when the data for penetrations 3, 4, and 6 were deleted from the 1981 data set, the results were as shown in figure 18. The comparisons improved, and the correlation coefficient increased from 0.47 to 0.78.

Figure 19 shows comparison plots for the 1980 and 1981 data combined. Data presented in figure 19(a) include all the thunderstorm penetrations, whereas the data presented in figure 19(b) exclude penetrations 3, 4, and 6 of the 1981 data. As might be expected, the comparisons were improved by excluding the three penetrations, and the correlation coefficient was increased from 0.78 to 0.88. Figure 19(b) may represent the best correlation that can be expected between Doppler radar and airplane data for similar experimental conditions as presented here. It is suggested, however, that several improvements in the experimental technique may improve the results. These improvements might include, for example, accounting for airplane position errors and making the airplane and radar measurements at the same time and close to the same position in space by slaving the radar to the airplane position. These improvements would properly locate the airplane position within the storm and minimize differences due to thunderstorm dynamics.

Concluding Remarks

A comparison of wind velocity measurements made in thunderstorms by an instrumented airplane and a ground-based Doppler radar was made. Comparisons were made for five airplane penetrations of two thunderstorms in 1980 and six penetrations of one thunderstorm in 1981. No attempt was made to achieve simultaneous or coextensive measurements, and consequently, an interpolation was necessary to match the two measurements in space and time. Correlation coefficients for the 1980 data and part of the 1981 data were 0.88 and 0.78, respectively. The correlation coefficient for this combined data set was 0.88. Some of the 1981 data showed large discrepancies between the airplane- and radar-measured data. Potential contributing factors for the discrepancies were identified and discussed. These correlations may represent the best that can be expected for this type of comparison, but it is suggested that improvements in the experimental technique would probably improve the results.

NASA Langley Research Center
Hampton, VA 23665
February 1, 1985

TABLE I. CHARACTERISTICS OF F-106B RESEARCH AIRPLANE

Length, m (ft)	21.54 (70.67)
Height, m (ft)	6.17 (20.25)
Wing span, m (ft)	11.70 (38.39)
Wing area (gross), m^2 (ft^2)	64.83 (697.82)
Wing chord at root, m (ft)	9.07 (29.77)
Aspect ratio	2.118
Wing sweepback angle	60°6′13″
Empty weight, N (lbf)	116 543 (26 200)
Gross take-off weight, N (lbf)	160 710 (36 129)
Engine	J75-P-17 axial flow turbojet
Thrust (military) at sea level, N (lbf)	71 616 (16 100)
Maximum thrust, N (lbf)	108 981 (24 500)

TABLE II. WIND AND TURBULENCE MEASUREMENTS ON F-106B AIRCRAFT INSTRUMENTATION SYSTEM

Measurement	Instrument range	1σ error	Resolution	Required flat to frequency response, Hz	Notes
Static pressure, psia*	0 to 15	0.07	0.0004	3	Quartz transducer—under nose Pitot-static head
Dynamic pressure, psi*	0 to 3	0.03	0.0004	6	Quartz transducer—nose boom for total pressure
Angle of attack, deg	±30	0.09	0.015	10	Flow vane on nose boom
Angle of sideslip, deg	±30	0.09	0.015	10	Flow vane on nose boom
Body rates, rad/s	±1	0.01	0.005	5	Mounted in weapons bay
Longitudinal and lateral acceleration, g units	±1	0.01	0.004	10	Mounted at center of gravity
Normal acceleration, g units	6 to −2	0.01	0.012	10	Mounted at center of gravity
Total air temperature, °C	35 to −75	0.03	0.205	0.5	Probe beneath nose
Pitch attitude, deg	±30	0.09	0.03	5	INS platform—continuous synchronization
Roll attitude, deg	±80	0.24	0.08	5	INS platform—continuous synchronization
Ground speed, m/s	±1248	0.9	0.0003	3	INS platform—digital
Latitude	±90°	1/60 deg/hr	0.14″	0.2	INS platform—digital
Longitude	±180°	1/60 deg/hr	0.14″	0.2	INS platform—digital
True heading	0° to 360°		0.14″	3	INS platform—digital
Vertical acceleration, g units	3 to −1	0.005	0.008	5	INS platform acceleration

*1 psi = 6.9 kPa.

TABLE III. NSSL DOPPLER RADAR CHARACTERISTICS

Antenna:	
Shape	Parabolic
Diameter, m	9.15
Half-power beam width, deg	0.81
Gain, dB	46.8
First side lobe level, dB	−21
Polarization	Vertical
Root-mean-square surface deviation, mm	2.8
Transmitter:	
Wavelength, cm	10.52
Frequency, MHz	2850
Peak power (typical), kW	750
Pulse width, μs (m)	1 (150)
Pulse repetition time (typical), μs	768
Receiver:	
System noise (typical),* dB	4
Transfer function	Doppler—linear Intensity—logarithmic
Dynamic range (typical), dB	80
Band width, MHz	
3 dB	0.60
6 dB	0.85
Noise power (typical), dBm	−108
Doppler time series data acquisition:	
No. of simultaneous range gates	16
No. of blocks along radial	8
Range gate spacing, m	150, 300, 600, 1200
Azimuthal sample spacing, deg	0.1 to 9.9
Automatic elevation increment, deg	0.1 to 9.9
No. of samples in time series	$2^n; n = 1, 2, ..., 13$
Complex video digital word length	12 bits (binary)
Mean velocity and spectrum width data acquisition:	
No. of range gates	762
Range gate spacing, m	150
No. of samples in estimate	$2^n; n = 5, 6, 7, 8$
Recorded word length	
Velocity	6 bits (2's complement)
Width	6 bits, 0–32 (binary)
Intensity data acquisition:	
No. of range gates	762
Range gate spacing, m	150, 600
No. of samples in estimate	$2^n - 1; 2^n; n = 3, 4$
Time window function	Linear or exponential
Recorded word length	6 bits (binary)

*Measured at receiver calibration port.

TABLE III. Concluded

General features:	
Azimuthal antenna rotation rate, deg/s	0.1 to 10
Maximum unambiguous range, km	115
Maximum unambiguous velocity (typical), ms^{-1}	±34.2
Plan-position indicator capability	Yes
Range-height indicator capability	Yes
Coplane capability	No
Calibration and timing:	
Radome loss (two-way), dB	2.0
Waveguide loss (two-way, from calibration port to antenna feed assembly), dB	2.0
Transmitter/receiver circulator loss (receiver port), dB	1.7
Receiver detection loss,† dB	2.7
Signal generator cable loss, dB	9.5
Directional coupler loss, dB	36.2
Delay to transmitter pulse,‡ μs	5.4
Pulse pair processor integrator delay,§ μs	3.5
Waveguide delay, μs	0.1
Doppler sample-hold aperture, μs	0.4
Doppler sample-hold time constant, μs	0.15
Pulse pair processor integrator sample-hold aperture, μs	0.04
Pulse pair processor integrator sample-hold time constant, μs	0.01
Receiver initial delay, μs	1.3
Receiver nominal delay, μs	1.8
Receiver rise time, μs	1.0

†See memo, "Reflectivity Equation for NSSL's WDS-71 10 cm Doppler Radar," Feb. 21, 1973, R. J. Doviak and D. Sirmans.

‡Delay from system pretrigger to first sample-hold operation.

§Pulse pair processor integrator delay—expanded, 6.5 μs.

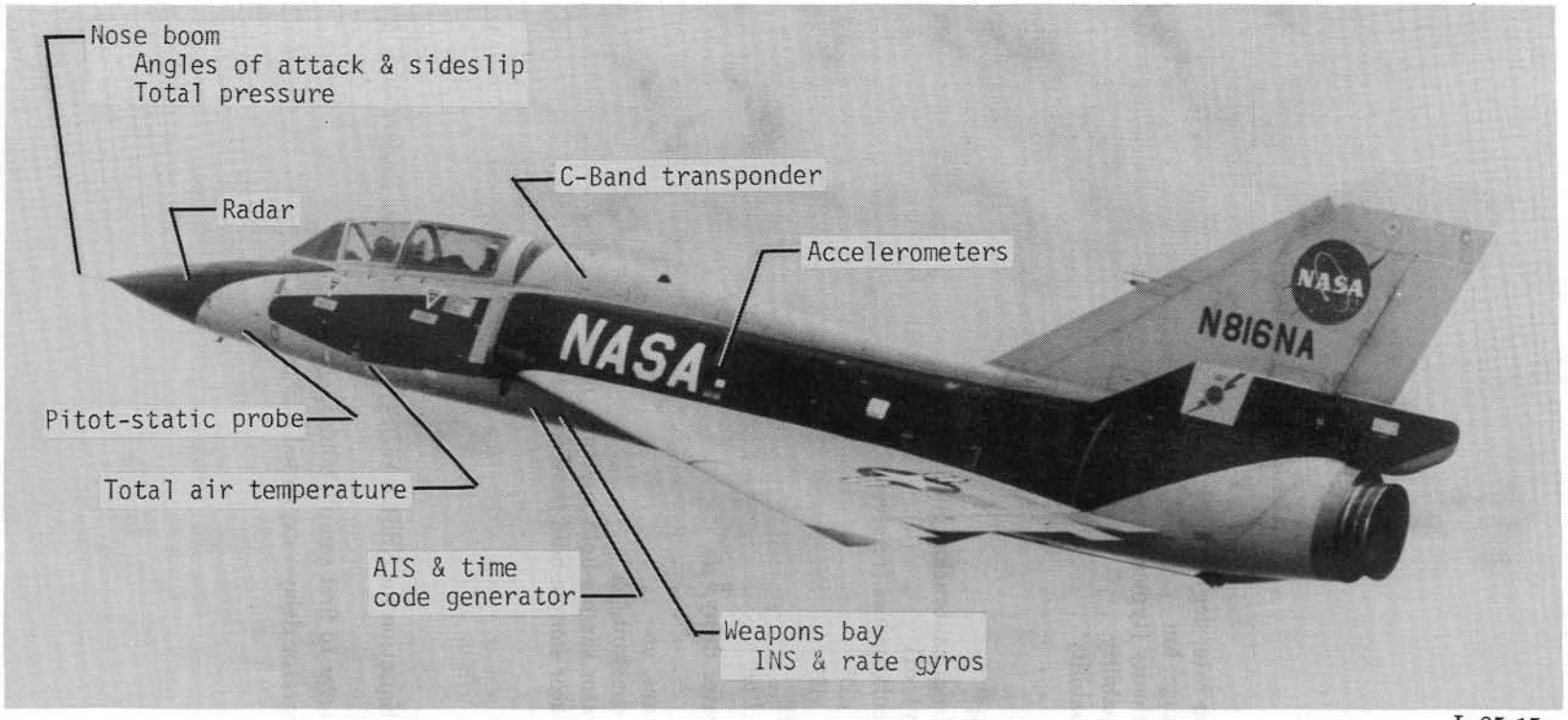

L-85-15

Figure 1. NASA F-106B research airplane used in Storm Hazards Program.

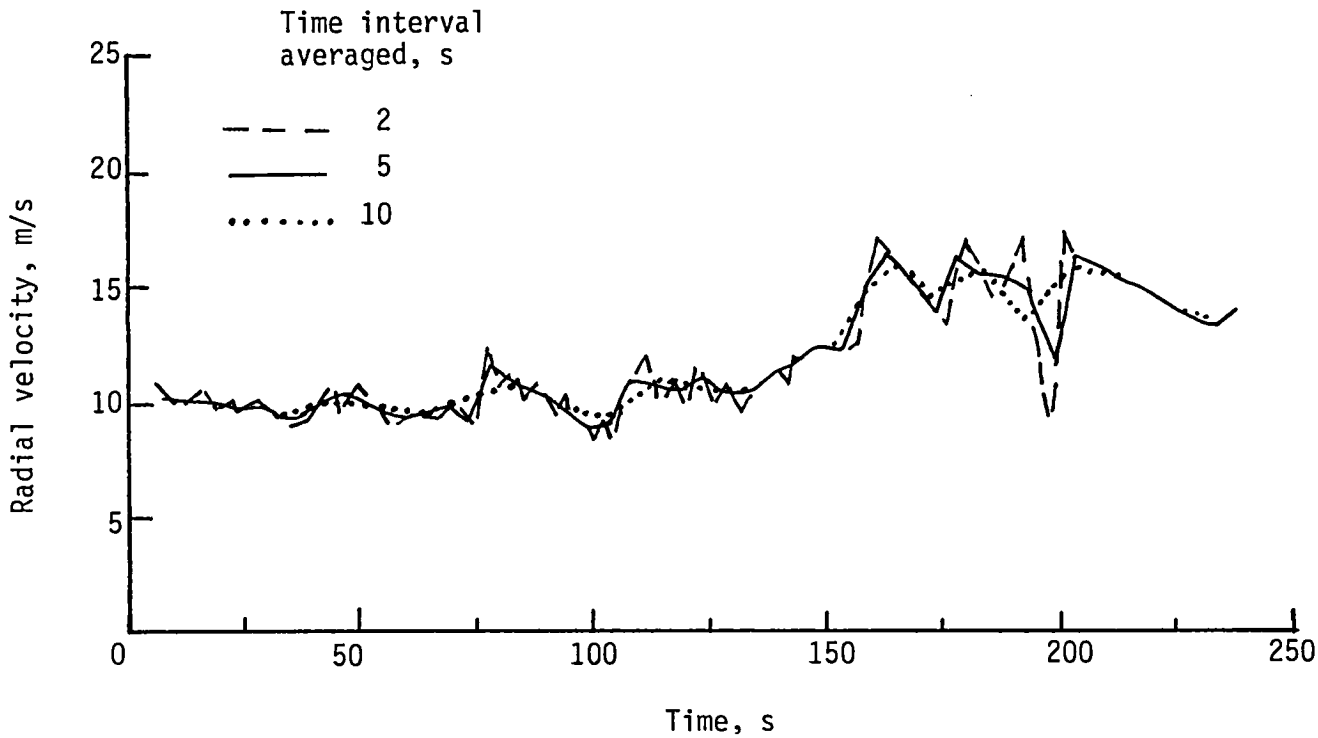

Figure 2. Typical radial velocity time histories derived from F-106B measurements with averaging intervals of 2, 5, and 10 s.

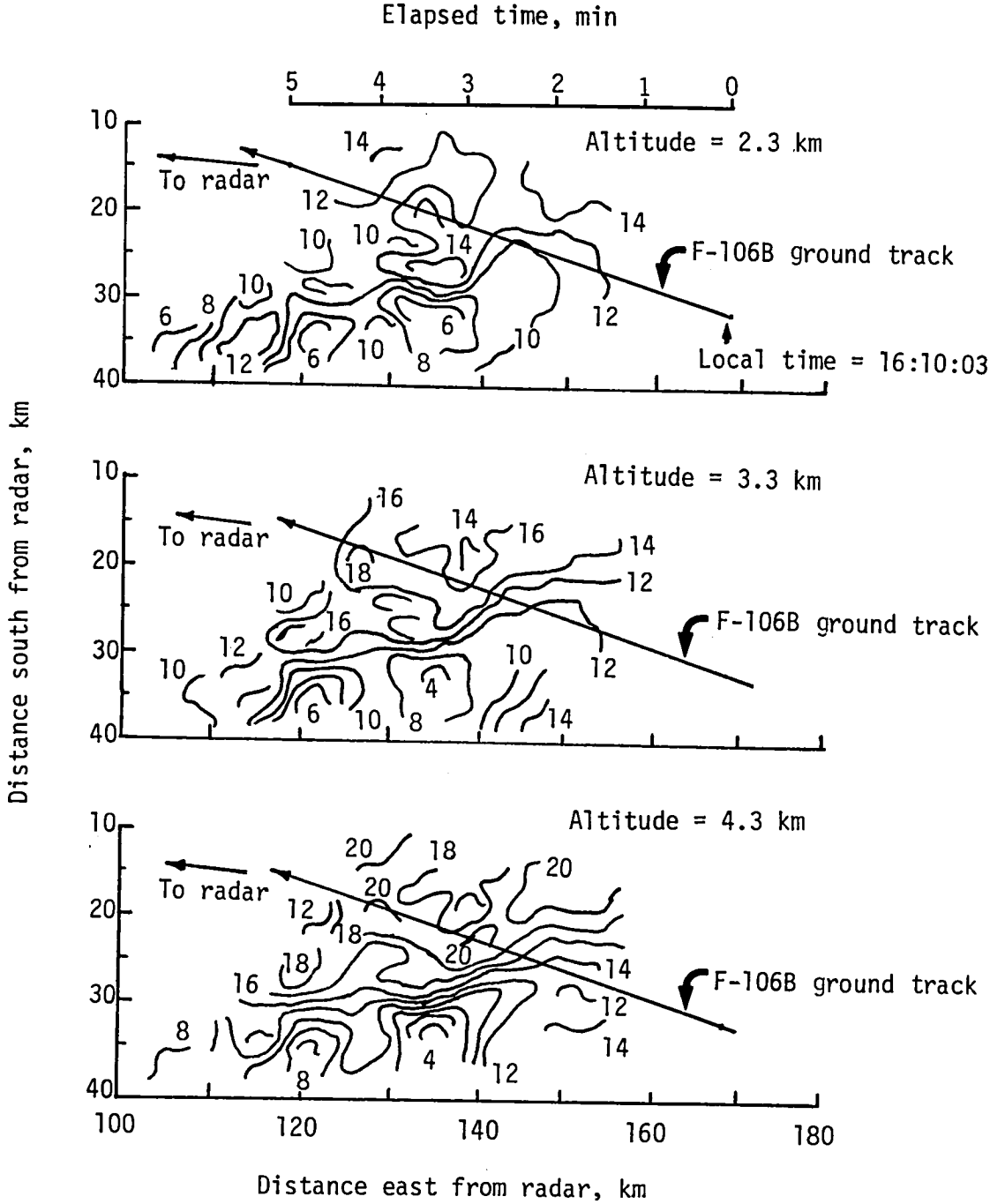

(a) F-106B ground track superimposed on Doppler radial velocity contours at three altitudes. Contours are labeled in meters per second.

Figure 3. Derivation of Doppler radar radial wind velocity at points along F-106B flight path by superposition and by interpolation between horizontal planes containing Doppler-measured radial velocity contours.

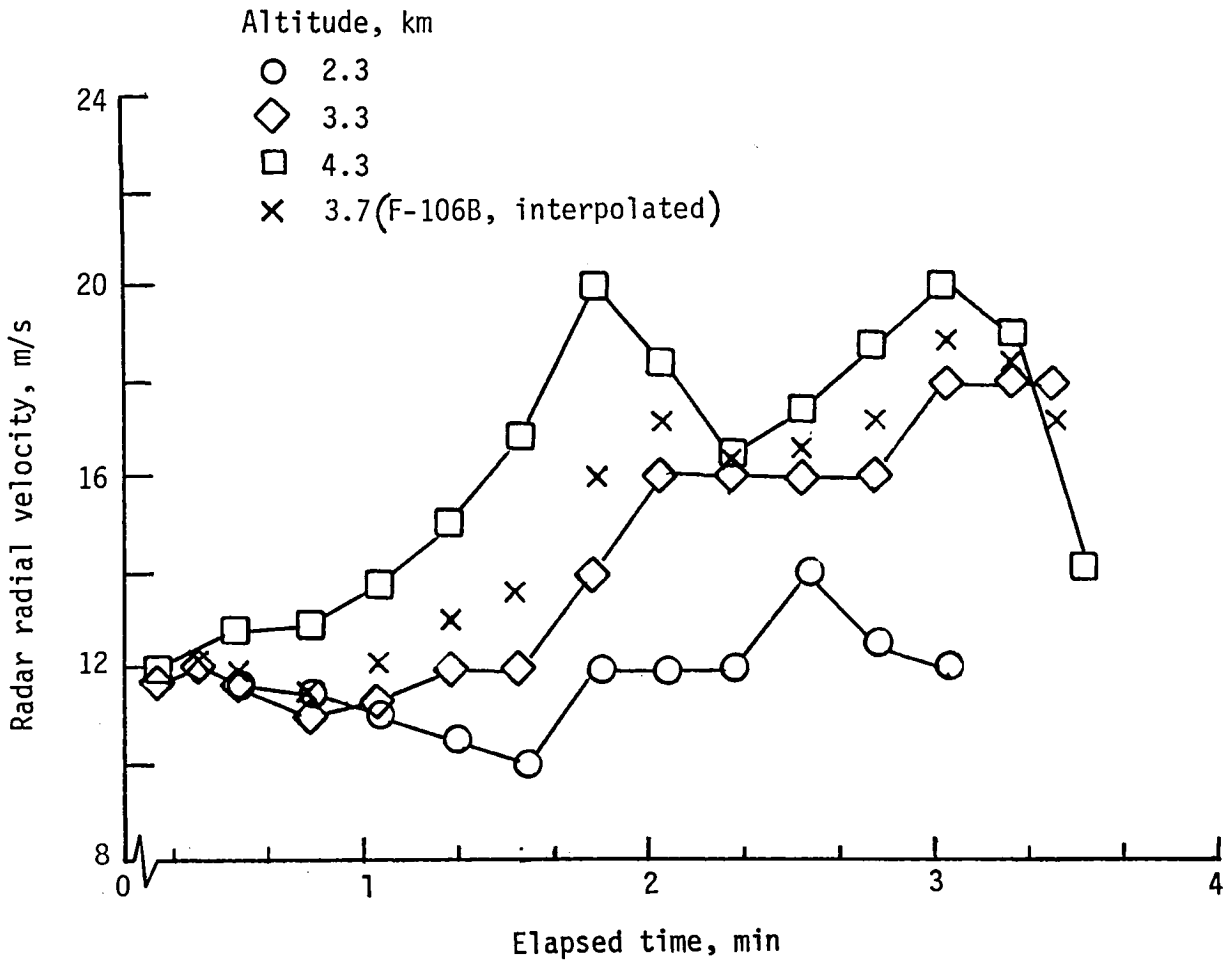

(b) Doppler radial velocity at points along F-106B flight path at three altitudes shown in figure 3(a) and at the F-106B altitude obtained by interpolation.

Figure 3. Concluded.

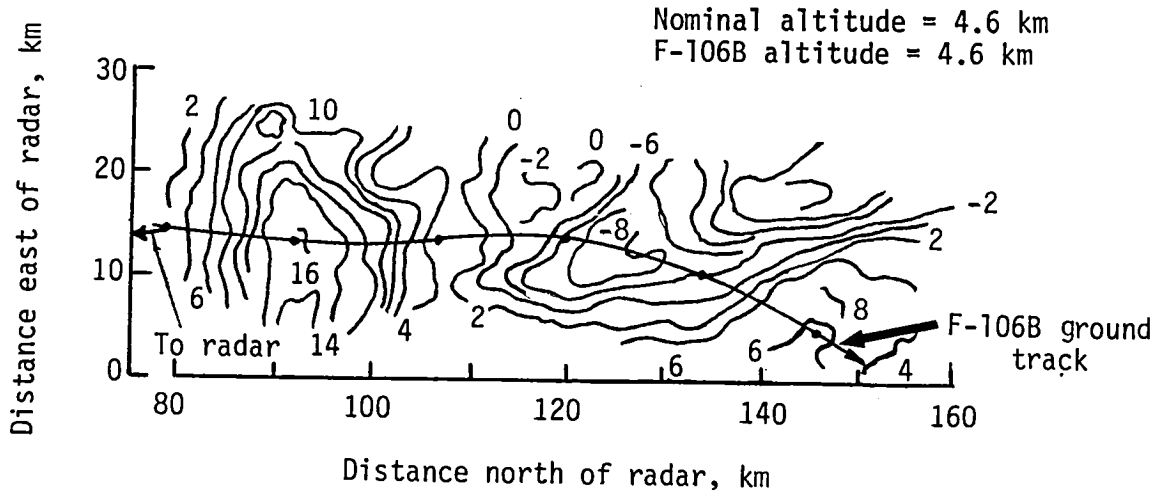

(a) Doppler radar radial velocity contours with F-106B ground track superimposed. Contours are labeled in meters per second.

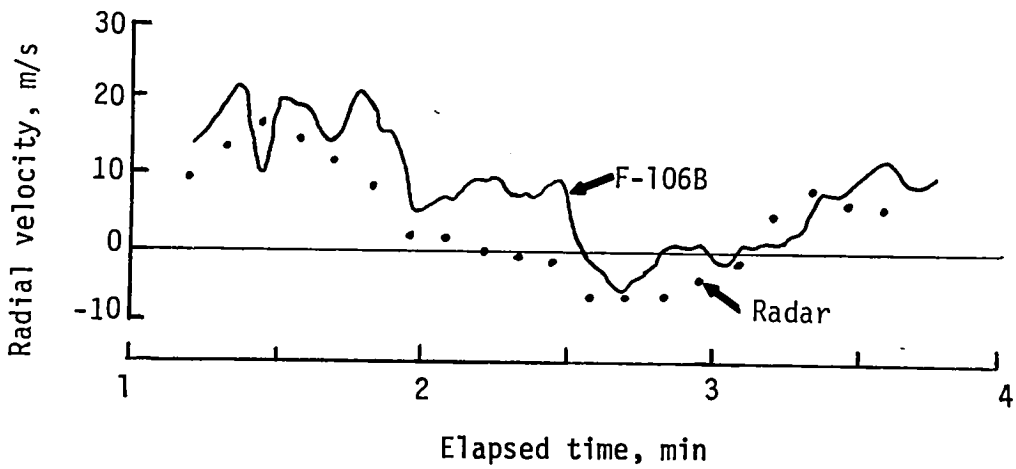

(b) Radial velocity.

Figure 4. F-106B ground track superimposed on Doppler radar radial velocity contours and radial velocity at points along flight path. Penetration 4; June 1980.

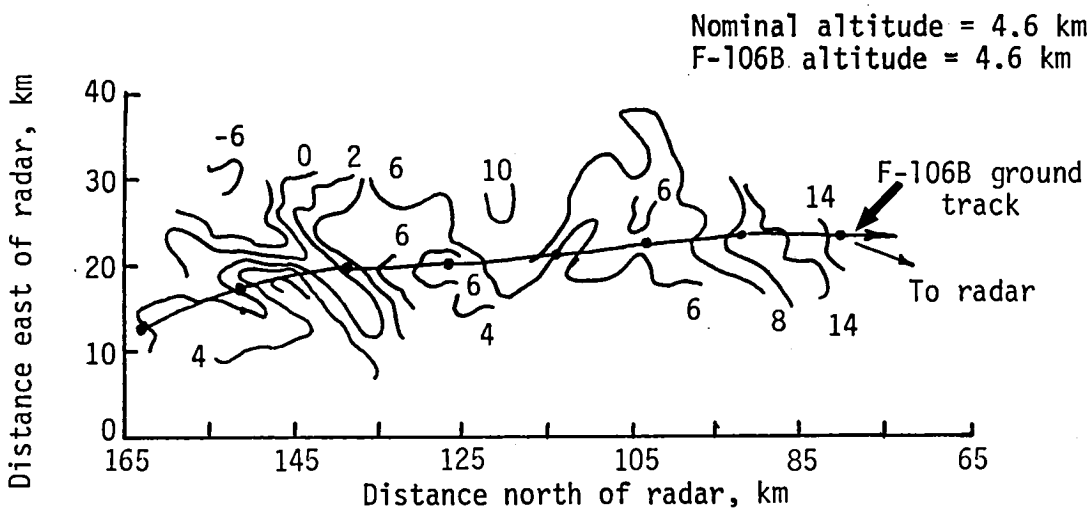

(a) Doppler radar radial velocity contours with F-106B ground track superimposed. Contours are labeled in meters per second.

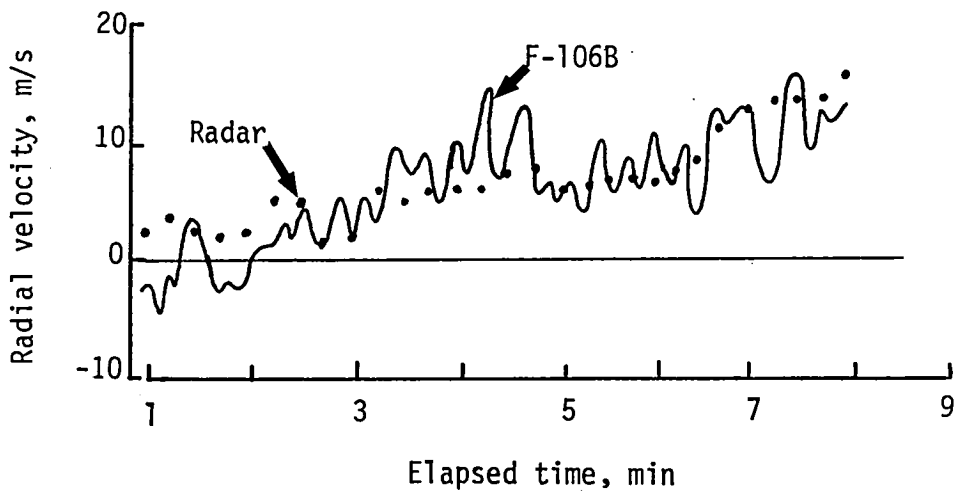

(b) Radial velocity.

Figure 5. F-106B ground track superimposed on Doppler radar radial velocity contours and radial velocity at points along flight path. Penetration 5; June 1980.

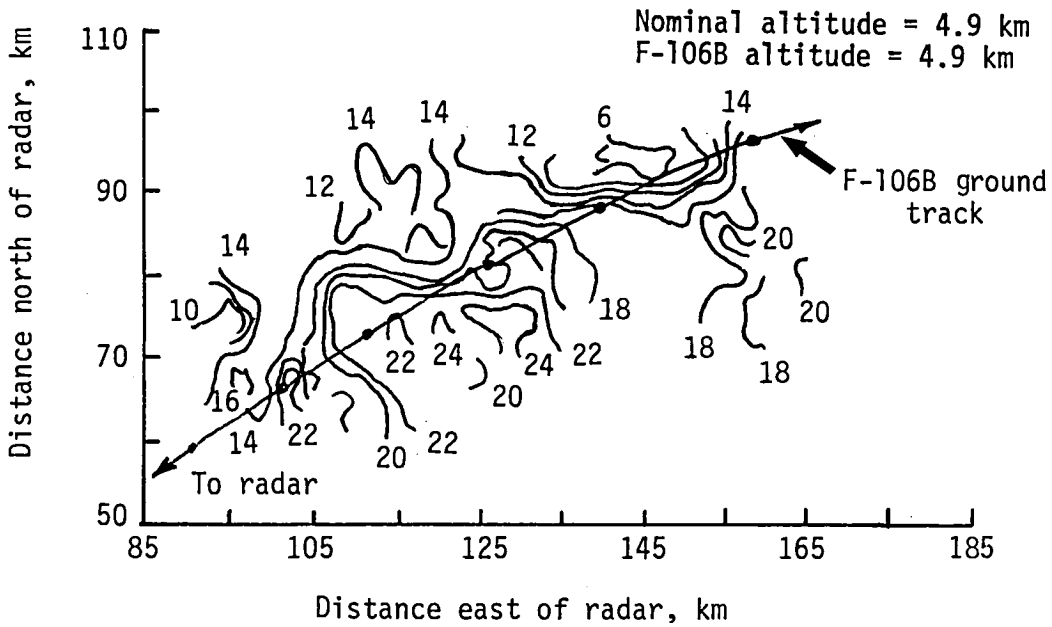

(a) Doppler radar radial velocity contours with F-106B ground track superimposed. Contours are labeled in meters per second.

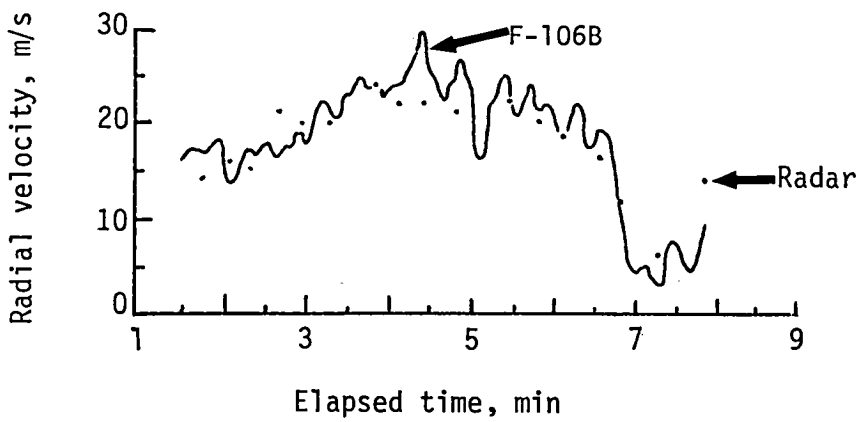

(b) Radial velocity.

Figure 6. F-106B ground track superimposed on Doppler radar radial velocity contours and radial velocity at points along flight path. Penetration 1; June 1980.

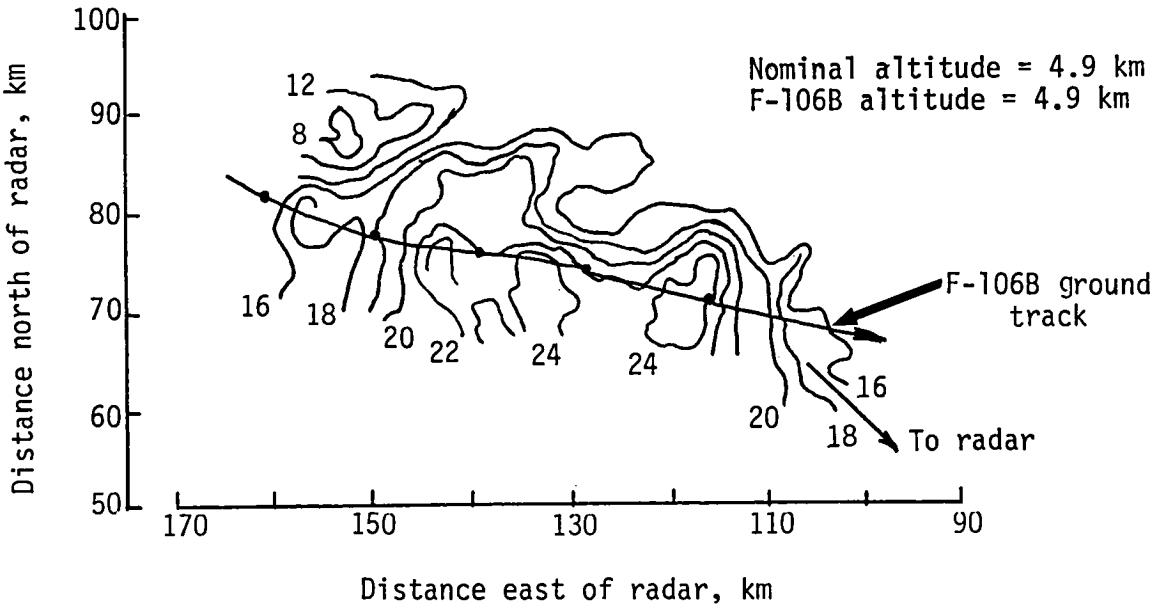

(a) Doppler radar radial velocity contours with F-106B ground track superimposed. Contours are labeled in meters per second.

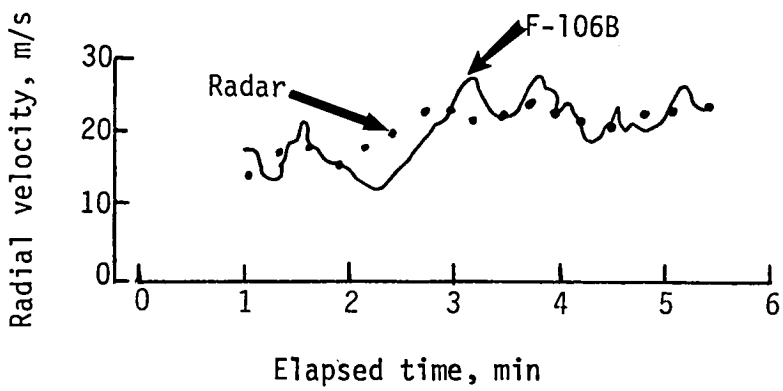

(b) Radial velocity.

Figure 7. F-106B ground track superimposed on Doppler radar radial velocity contours and radial velocity at points along flight path. Penetration 2; June 1980.

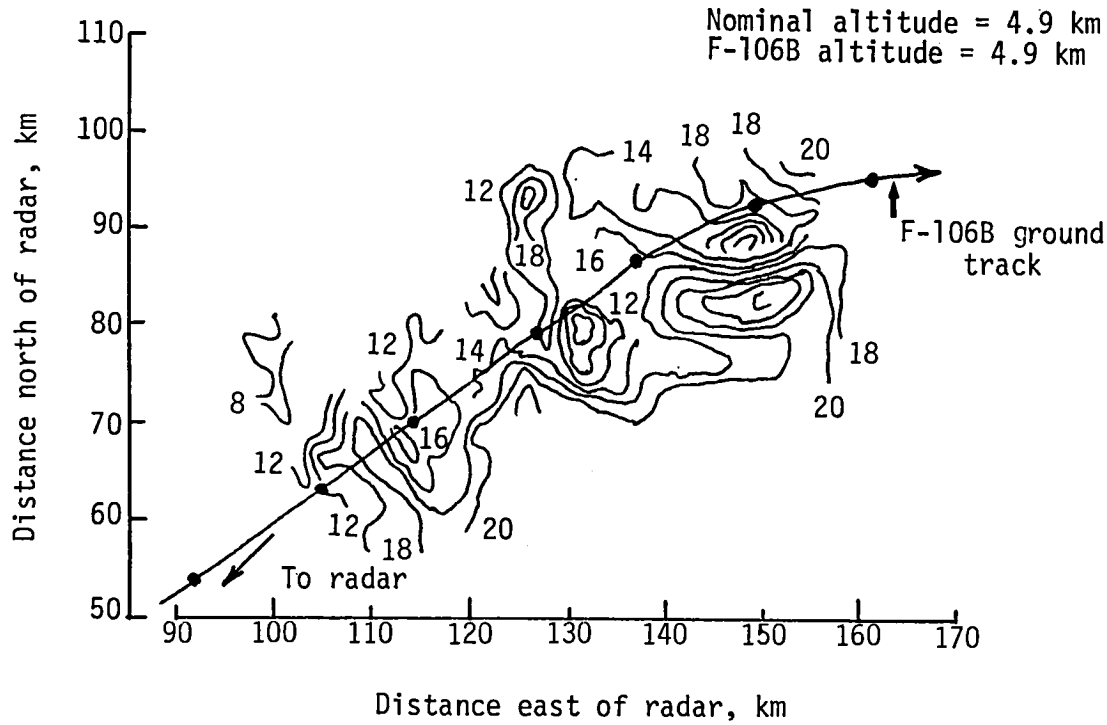

(a) Doppler radar radial velocity contours with F-106B ground track superimposed. Contours are labeled in meters per second.

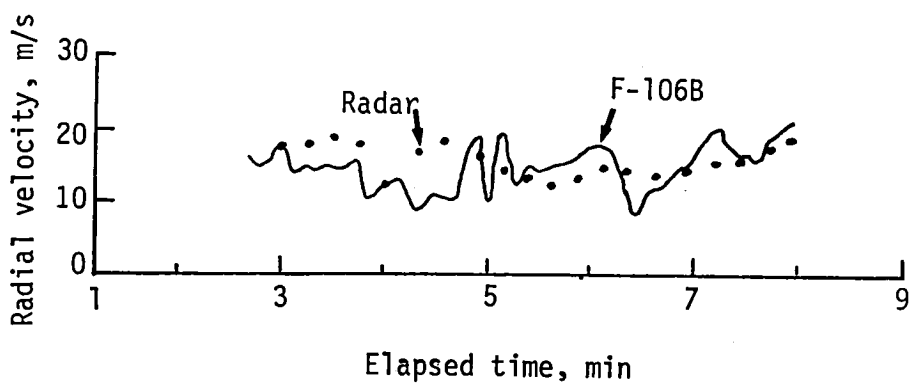

(b) Radial velocity.

Figure 8. F-106B ground track superimposed on Doppler radar radial velocity contours and radial velocity at points along flight path. Penetration 3; June 1980.

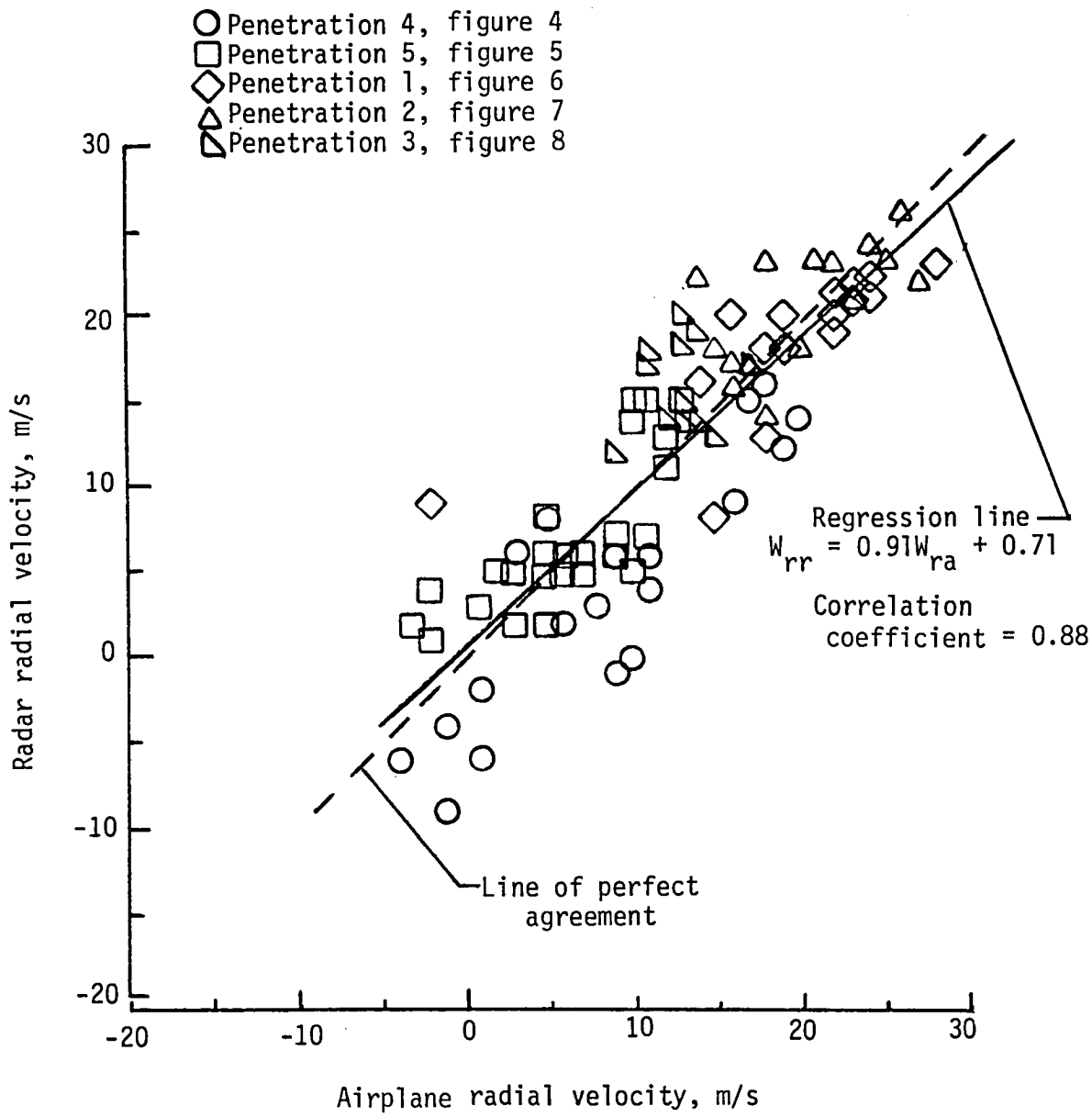

Figure 9. Comparison of Doppler radar and F-106B radial velocity data from June 1980.

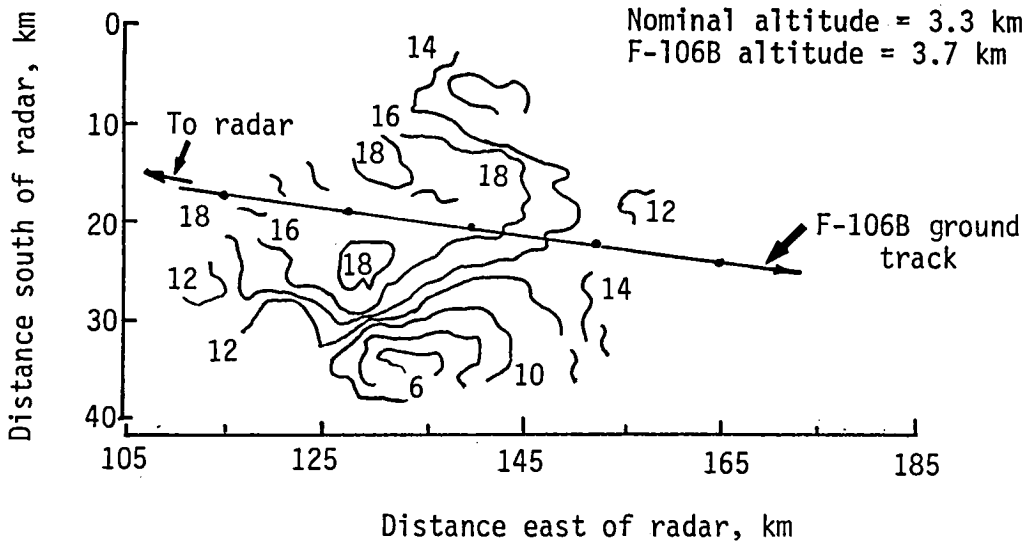

(a) Doppler radar radial velocity contours with F-106B ground track superimposed. Contours are labeled in meters per second.

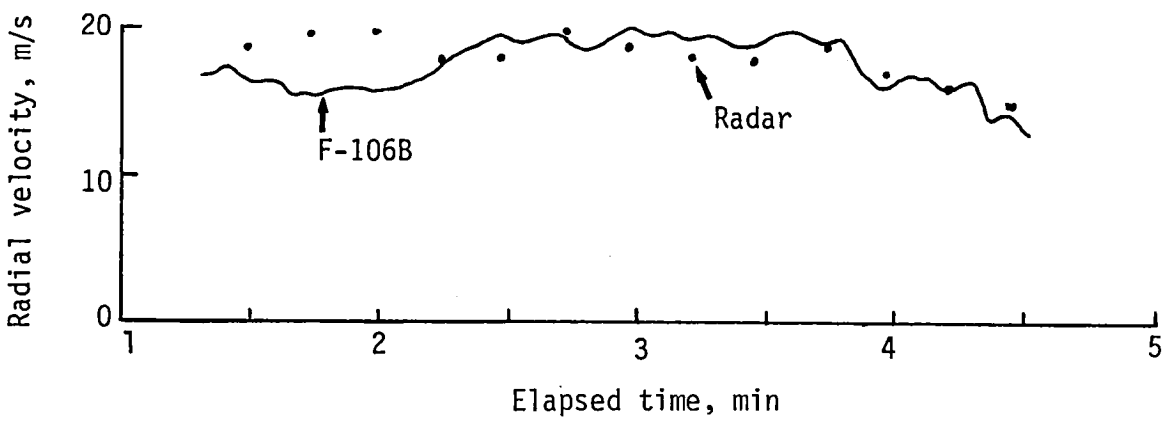

(b) Radial velocity.

Figure 10. F-106B ground track superimposed on Doppler radar radial velocity contours and radial velocity at points along flight path. Penetration 1; April 1981.

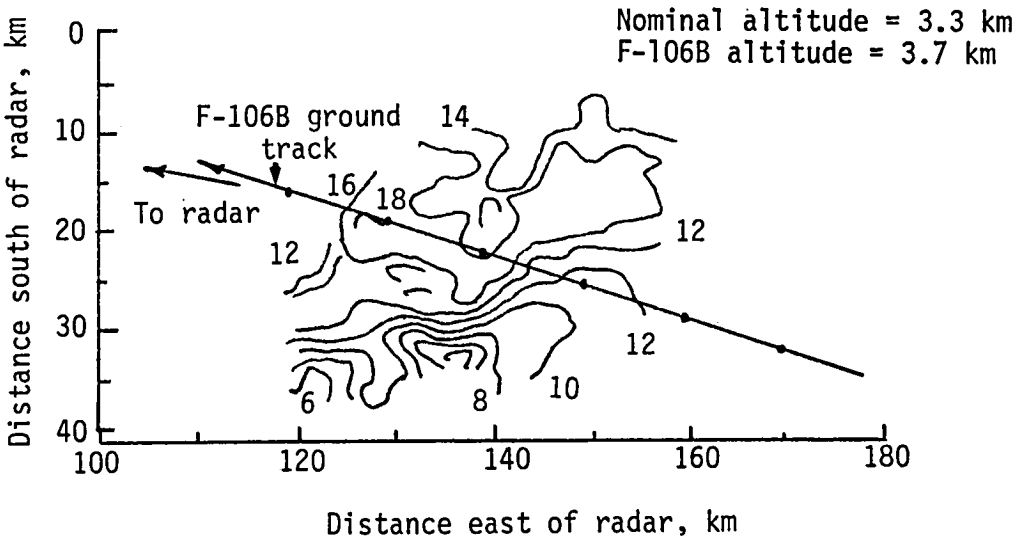

(a) Doppler radar radial velocity contours with F-106B ground track superimposed. Contours are labeled in meters per second.

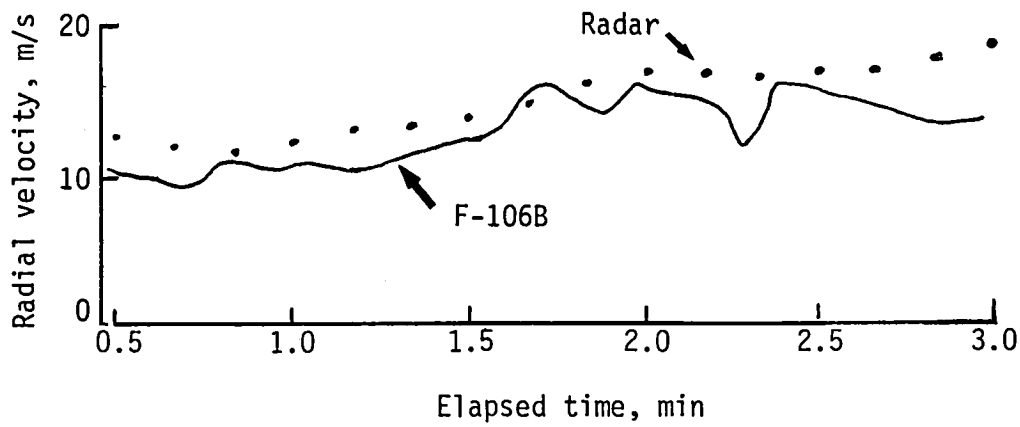

(b) Radial velocity.

Figure 11. F-106B ground track superimposed on Doppler radar radial velocity contours and radial velocity at points along flight path. Penetration 2; April 1981.

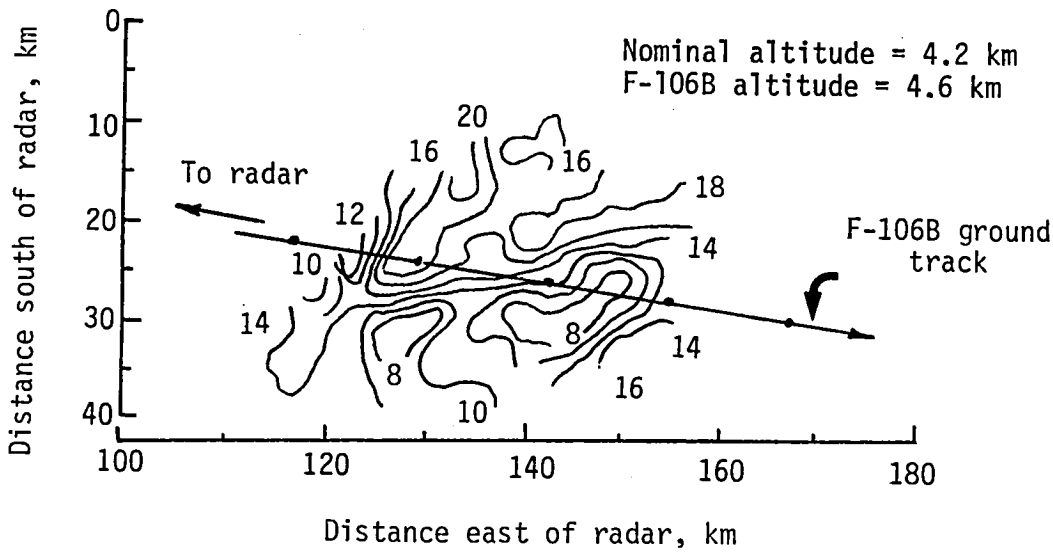

(a) Doppler radar radial velocity contours with F-106B ground track superimposed. Contours are labeled in meters per second.

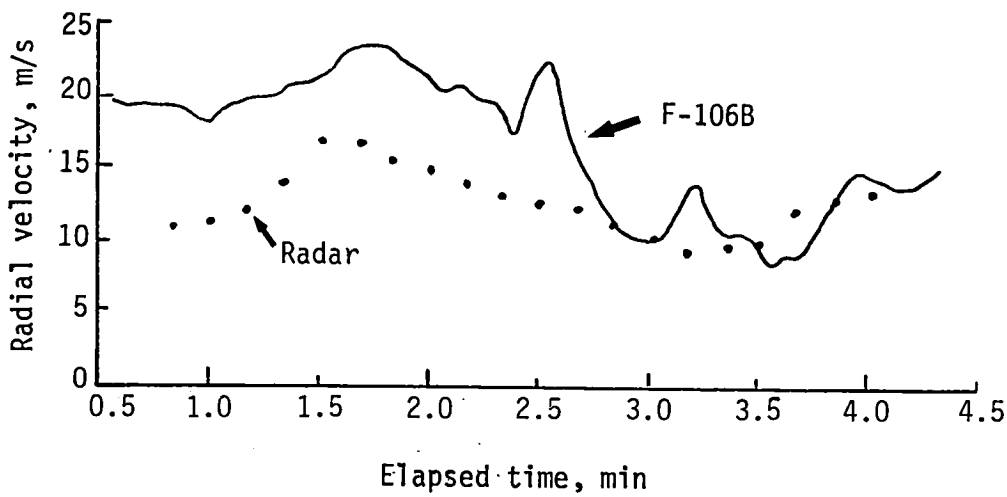

(b) Radial velocity.

Figure 12. F-106B ground track superimposed on Doppler radar radial velocity contours and radial velocity at points along flight path. Penetration 3; April 1981.

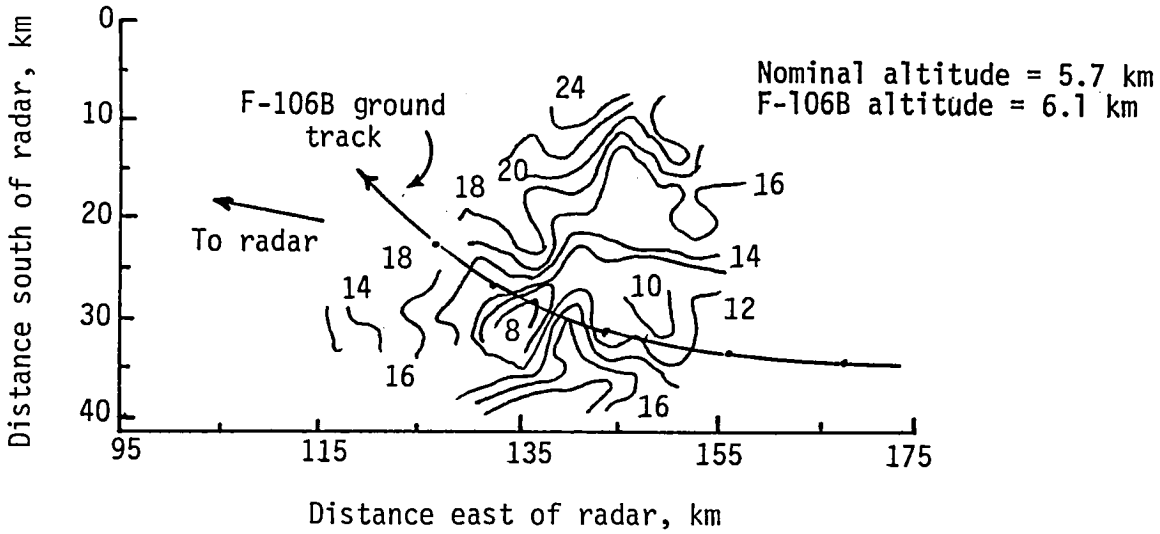

(a) Doppler radar radial velocity contours with F-106B ground track superimposed. Contours are labeled in meters per second.

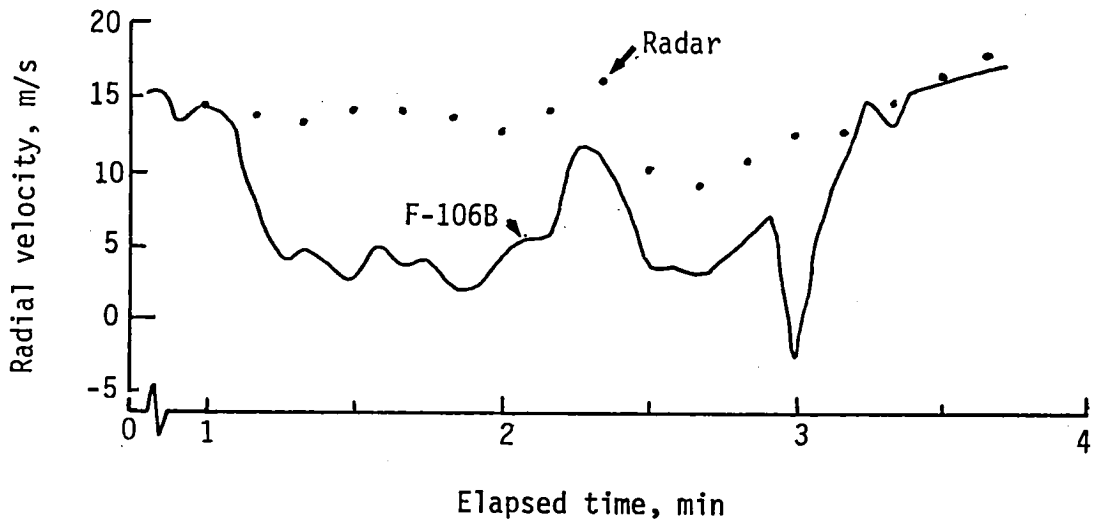

(b) Radial velocity.

Figure 13. F-106B ground track superimposed on Doppler radar radial velocity contours and radial velocity at points along flight path. Penetration 4; April 1981.

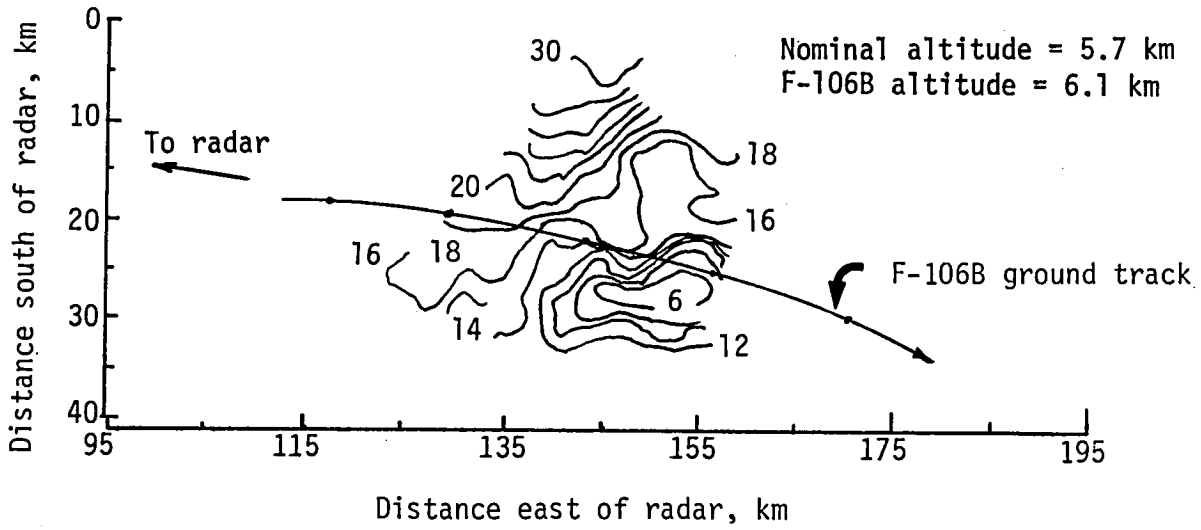

(a) Doppler radar radial velocity contours with F-106B ground track superimposed. Contours are labeled in meters per second.

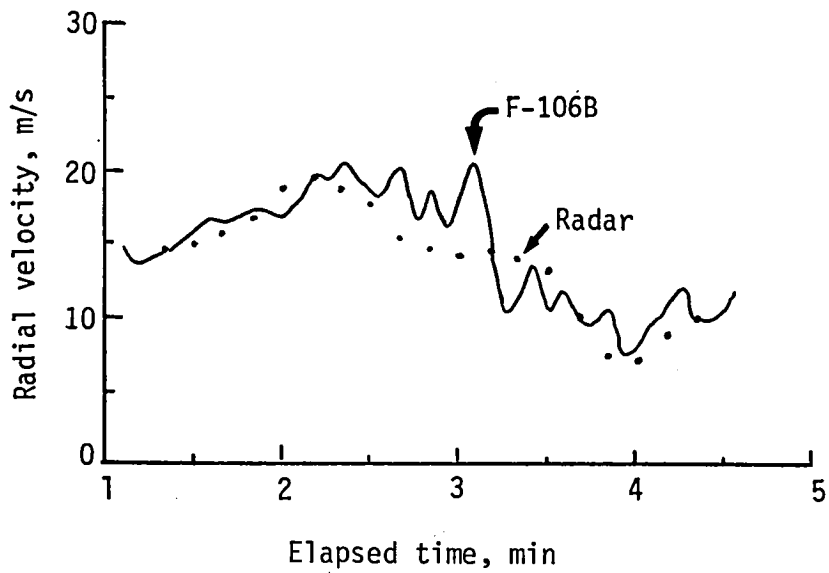

(b) Radial velocity.

Figure 14. F-106B ground track superimposed on Doppler radar radial velocity contours and radial velocity at points along flight path. Penetration 5; April 1981.

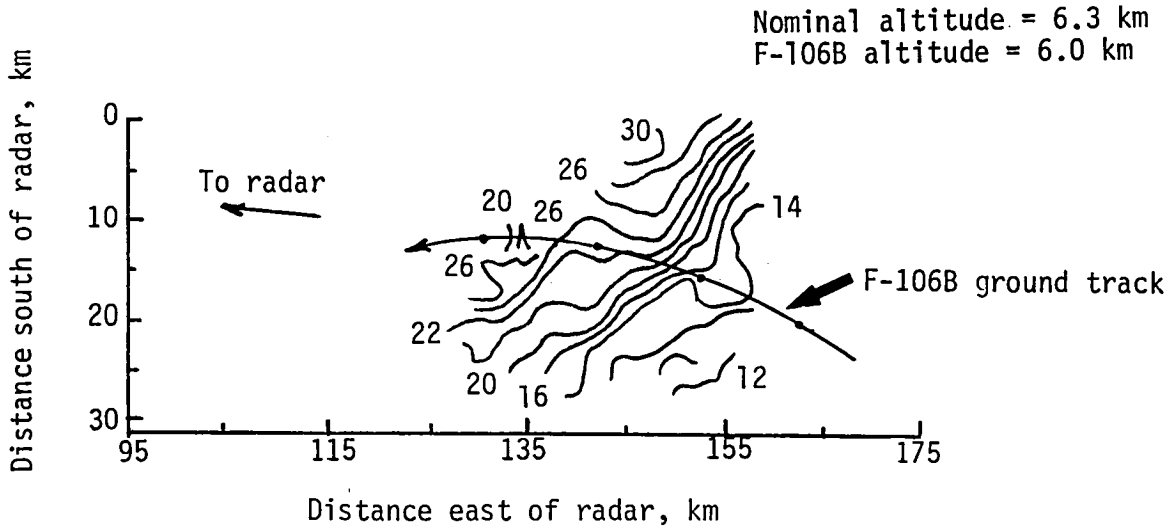

(a) Doppler radar radial velocity contours with F-106B ground track superimposed. Contours are labeled in meters per second.

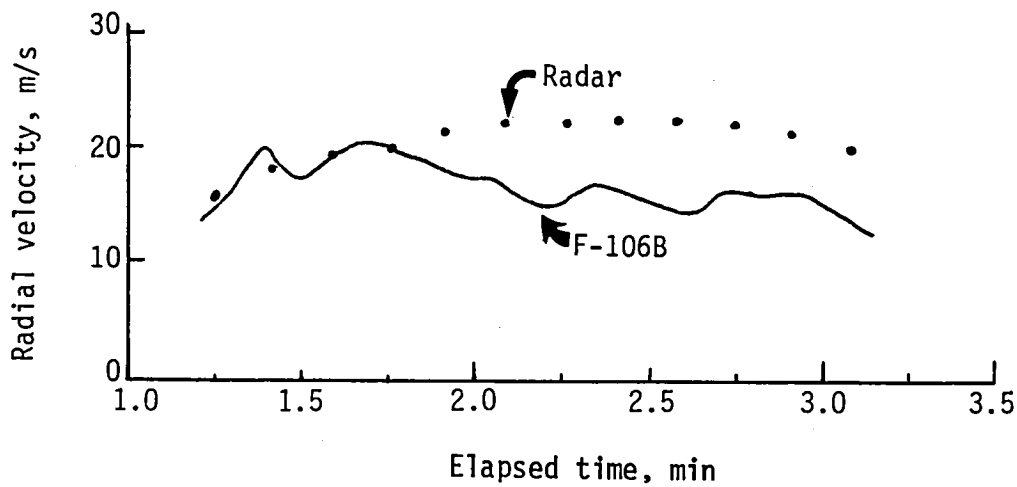

(b) Radial velocity.

Figure 15. F-106B ground track superimposed on Doppler radar radial velocity contours and radial velocity at points along flight path. Penetration 6; April 1981.

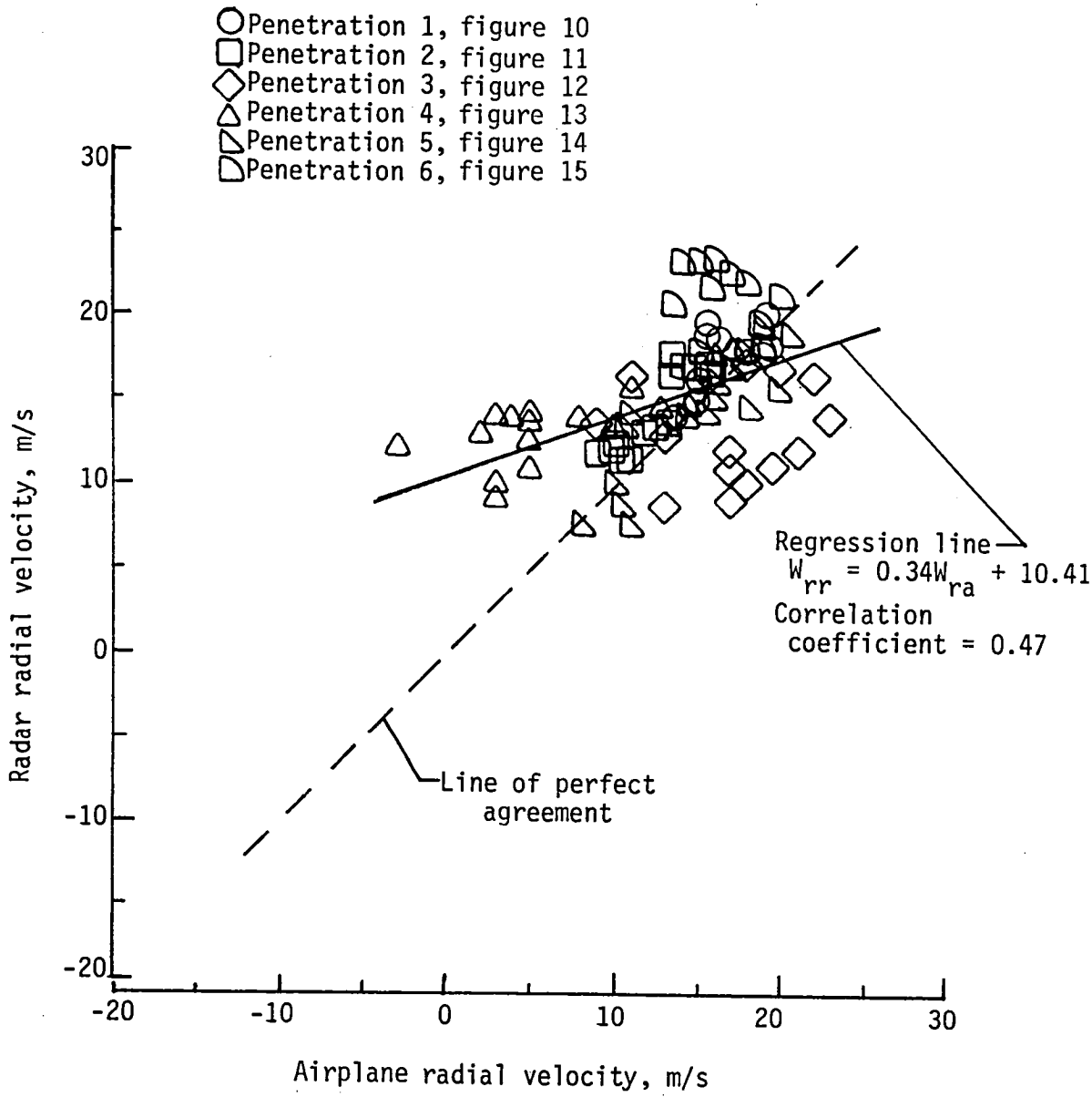

Figure 16. Comparison of Doppler radar and F-106B radial velocity data from April 1981.

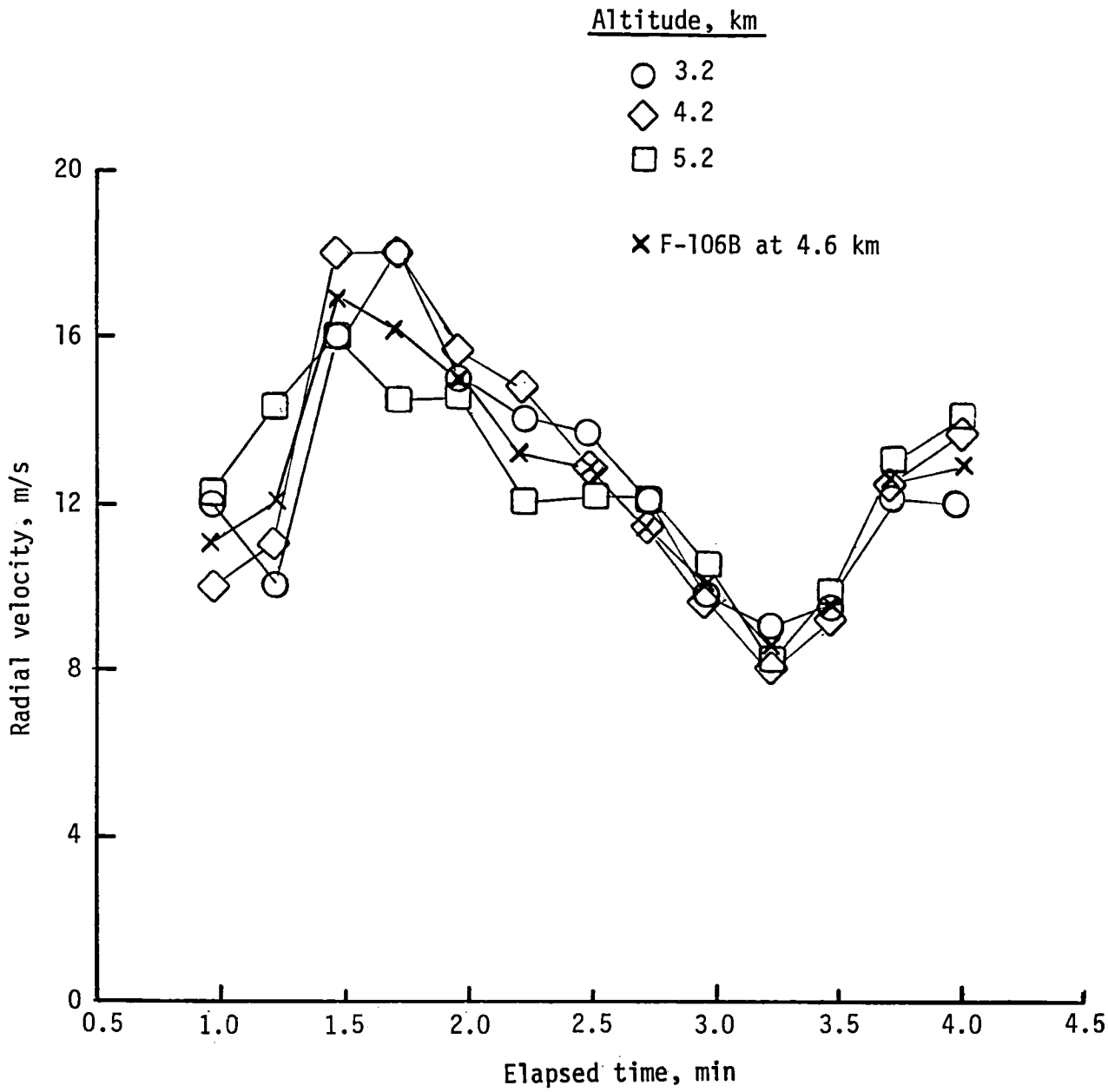

(a) Penetration 3; April 1981.

Figure 17. Doppler radar radial velocity at three altitudes for three passes through thunderstorm.

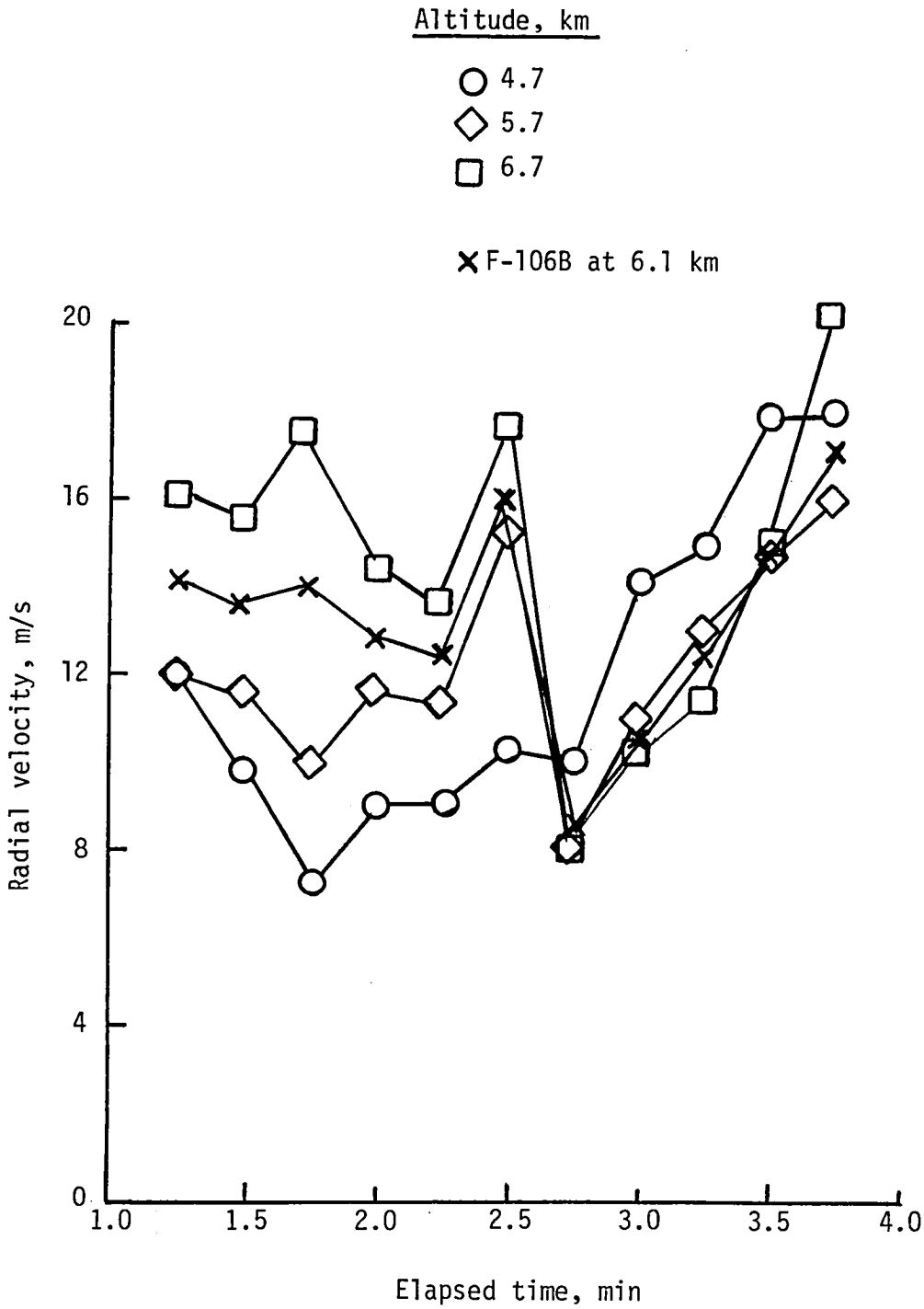

(b) Penetration 4; April 1981.

Figure 17. Continued.

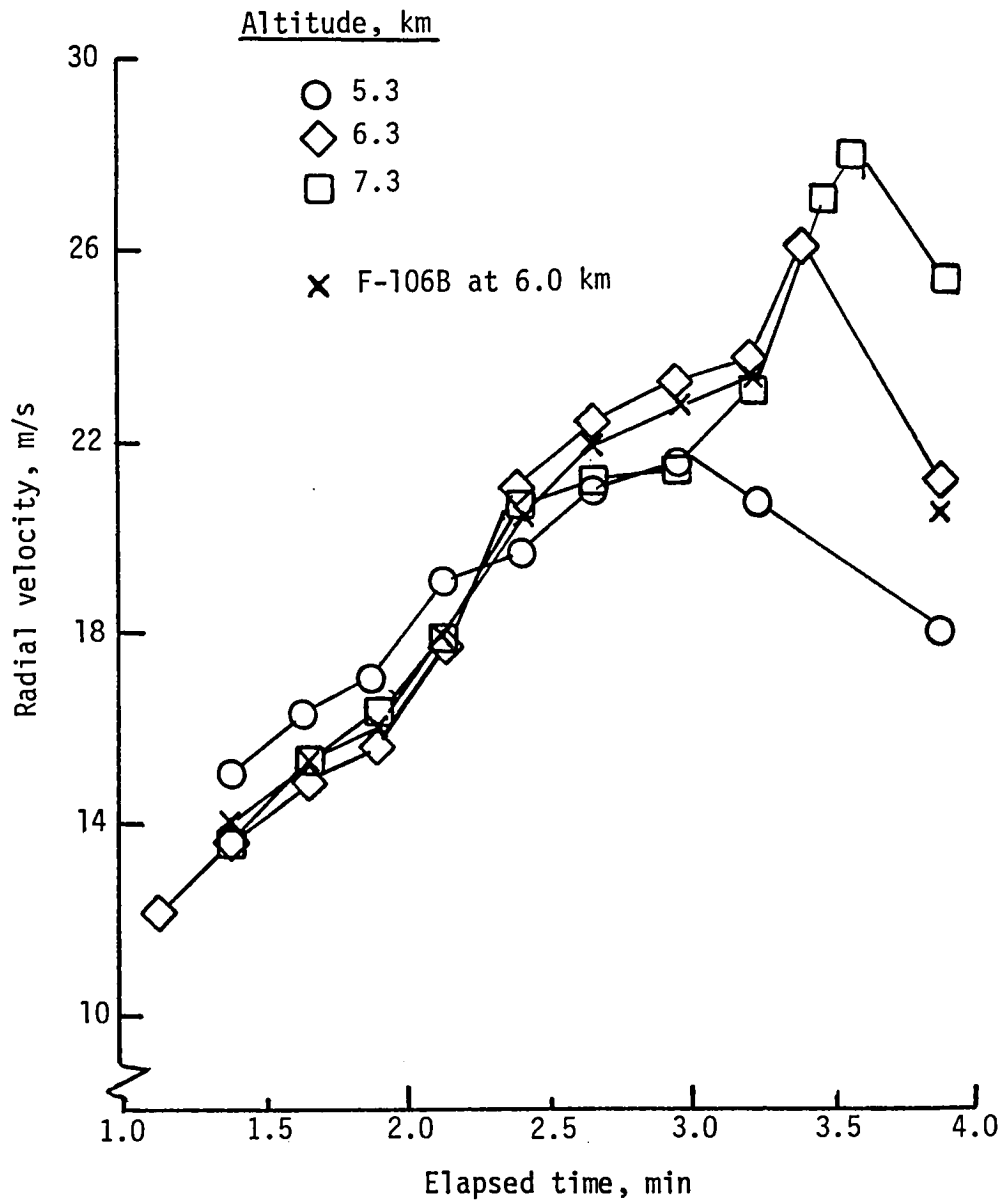

(c) Penetration 6; April 1981.

Figure 17. Concluded.

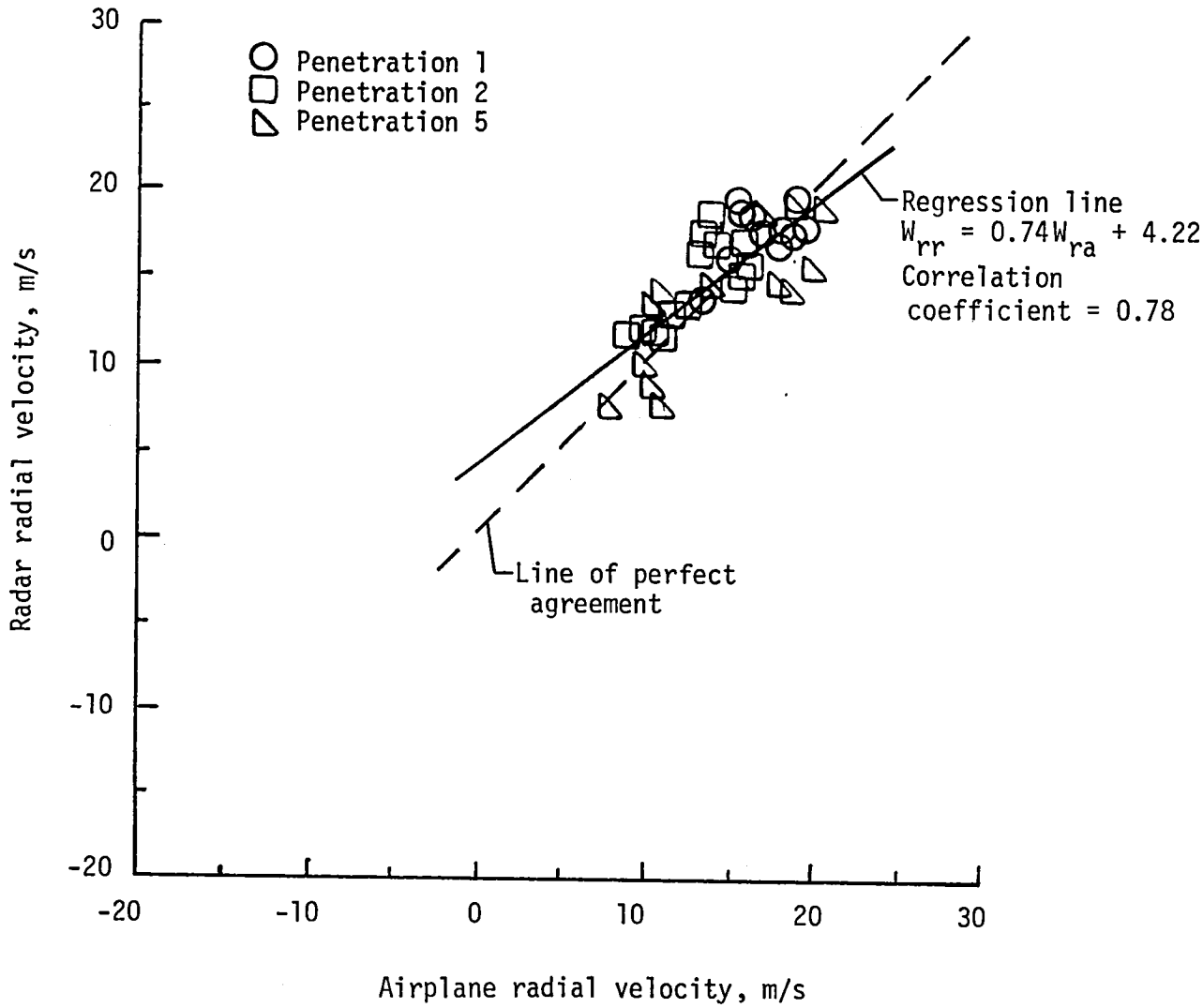

Figure 18. Comparison of Doppler radar and F-106B radial velocity data from April 1981 excluding penetrations 3, 4, and 6. (See fig. 16.)

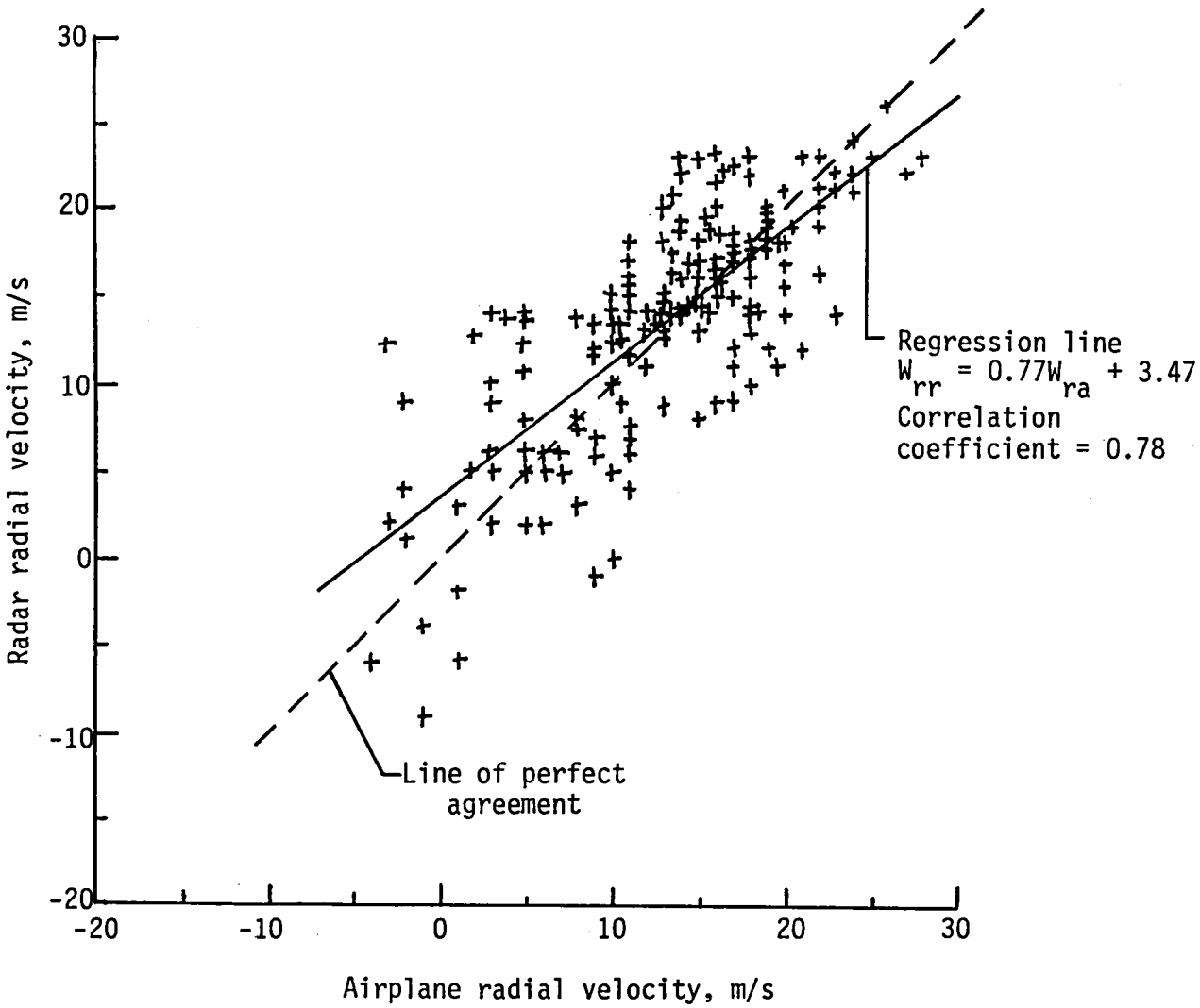

(a) Includes all penetrations for 1980 and 1981.

Figure 19. Comparison of Doppler radar and F-106B radial velocity data for 1980–1981.

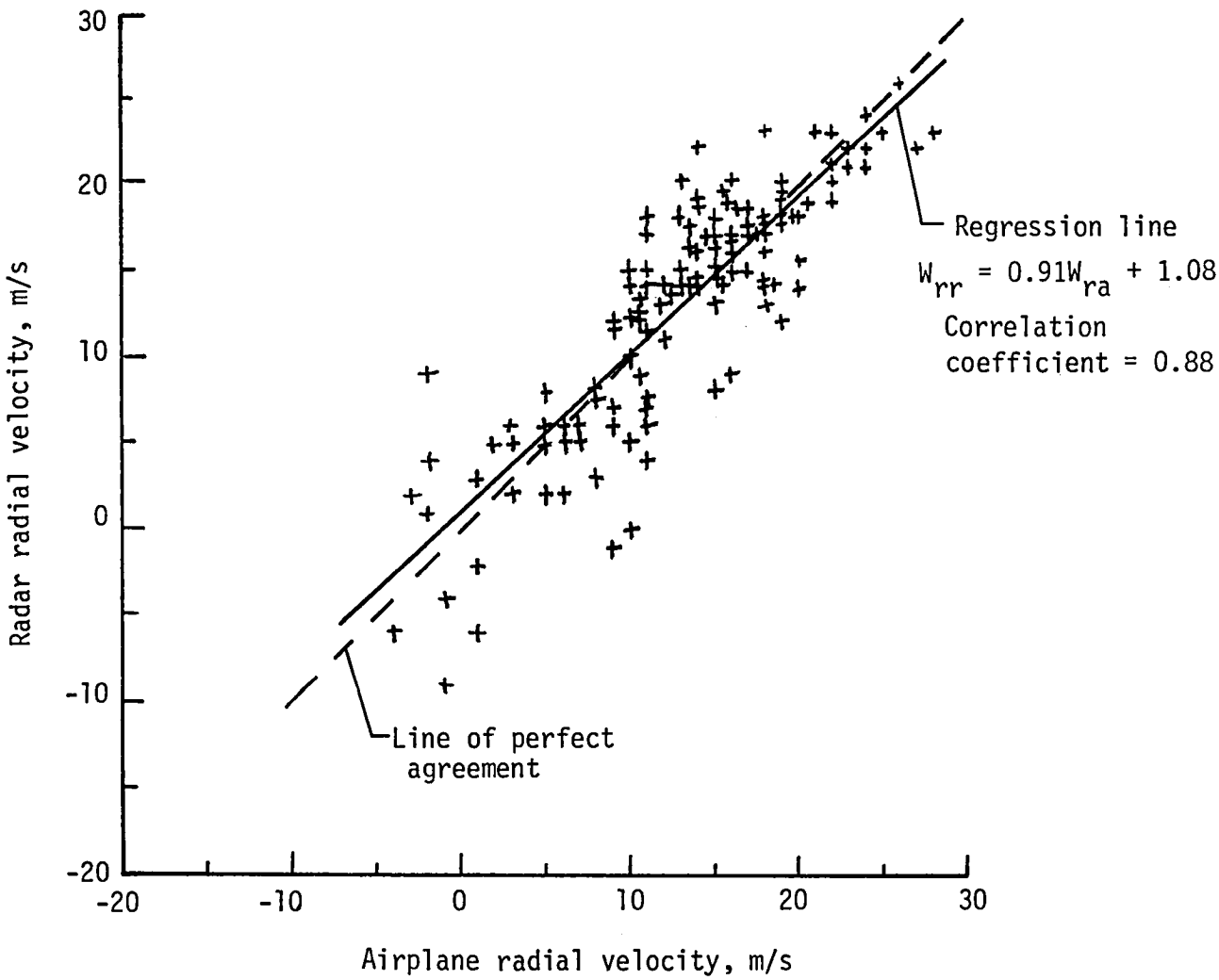

(b) Excludes penetrations 3, 4, and 6 of the 1981 data.

Figure 19. Concluded.

Appendix

Determination of Radial Wind Velocity From Airplane Measurements

The wind vector was determined by subtracting the F-106B air mass relative velocity from the inertial velocity by

$$\mathbf{W} = \mathbf{V}_I - \mathbf{V} \tag{A1}$$

where the inertial components were calculated from (fig. A1)

$$\begin{Bmatrix} W_{x'} \\ W_{y'} \\ W_{z'} \end{Bmatrix} = \begin{Bmatrix} V_{x'} \\ V_{y'} \\ V_{z'} \end{Bmatrix} - \Gamma \begin{Bmatrix} \mathbf{V}\cos\alpha\cos\beta \\ \mathbf{V}\sin\beta\cos\alpha \\ \mathbf{V}\sin\alpha \end{Bmatrix} - \Gamma \begin{Bmatrix} 0 \\ lr \\ lq \end{Bmatrix} \tag{A2}$$

and

$$\Gamma = \begin{bmatrix} \cos\psi\cos\theta & \sin\theta\sin\phi\cos\psi - \sin\psi\cos\phi & \cos\psi\cos\phi\sin\theta + \sin\psi\sin\phi \\ \cos\theta\sin\psi & \sin\psi\sin\theta\sin\phi + \cos\psi\cos\phi & \sin\psi\cos\phi\sin\theta - \cos\psi\sin\phi \\ -\sin\theta & \sin\phi\cos\theta & \cos\phi\cos\theta \end{bmatrix} \tag{A3}$$

The matrix Γ transforms measurements in the F-106B body-axis system to an Earth-fixed or inertial axis system. (See ref. 10.) The component of $\mathbf{W}$ in the direction of the Doppler radar is (fig. A1)

$$W_r = \mathbf{W} \cdot \mathbf{a} \tag{A4}$$

In equation (A2), airspeed was determined from measurements of pitot-static pressure and air temperature corrected for Mach number effects. The pitot-static tube was calibrated by the method in reference 11. Position effects were removed based on inflight measurements and the ground-camera flyby method also described in reference 11. The calibration curve for static pressure is shown in figure A2. In figure A2 the difference between the measured static pressure and the correct static pressure (Δp_s) normalized by the measured dynamic pressure is plotted as a function of measured angle of attack. The corrected static pressure and measured dynamic pressure are used in the isentropic perfect-gas-flow equation to determine Mach number. The measured total temperature, Mach number, and instrument correction recovery factor were used to determine static temperature from the adiabatic perfect-gas-flow relationship. True airspeed is determined from Mach number and the acoustic velocity as determined from static temperature. (See ref. 11.)

Laminated balsa flow vanes (described in ref. 12) were used for measuring sideslip angle and angle of attack. Flight test calibrations were conducted to correct the measured angle of attack for upwash effects. These data consisted of comparing the measured angle of attack with the pitch attitude while in a steady, level flight over the airspeed calibration range under the assumption of small vertical air mass velocities. A second-order least-squares error fit to the flight data yielded the following correction for angle of attack in degrees:

$$\alpha = 0.89506\alpha_m - 0.47952 \tag{A5}$$

Flow-field corrections for angle of sideslip were not used. The vanes were located in the symmetrical lateral plane and far enough ahead of the airplane that sidewash corrections were assumed to be small. For these flights, the natural frequency of the vanes was estimated at about 40 Hz. The measured natural frequency of the nose boom was 20 Hz. To prevent aliasing, the α and β measurements were filtered before they were digitized with a low-pass filter having a cutoff frequency of 10 Hz.

The inertial horizontal velocity components in equation (A2) were outputs of the INS. The vertical component was determined by integrating the vertical INS acceleration where

$$V_{z'} = -9.807 \int_0^t A_z\, dt + (V_{z'})_0 \tag{A6}$$

The constant (9.807) converts g units to meters per second squared. The symbol $(V_{z'})_0$ represents the initial vertical velocity, which was determined by equating the integrated vertical velocity to the pressure altitude change occurring over a time interval T of interest, i.e.,

$$\Delta h_p(T) = h_p(T) - h_p(0) = -\int_0^t V_{z'}\, dt \tag{A7}$$

and

$$(V_{z'})_0 = \frac{1}{T}\left[-\Delta h_p(T) + 9.807 \int_0^t \int A_z\, dt\right] \tag{A8}$$

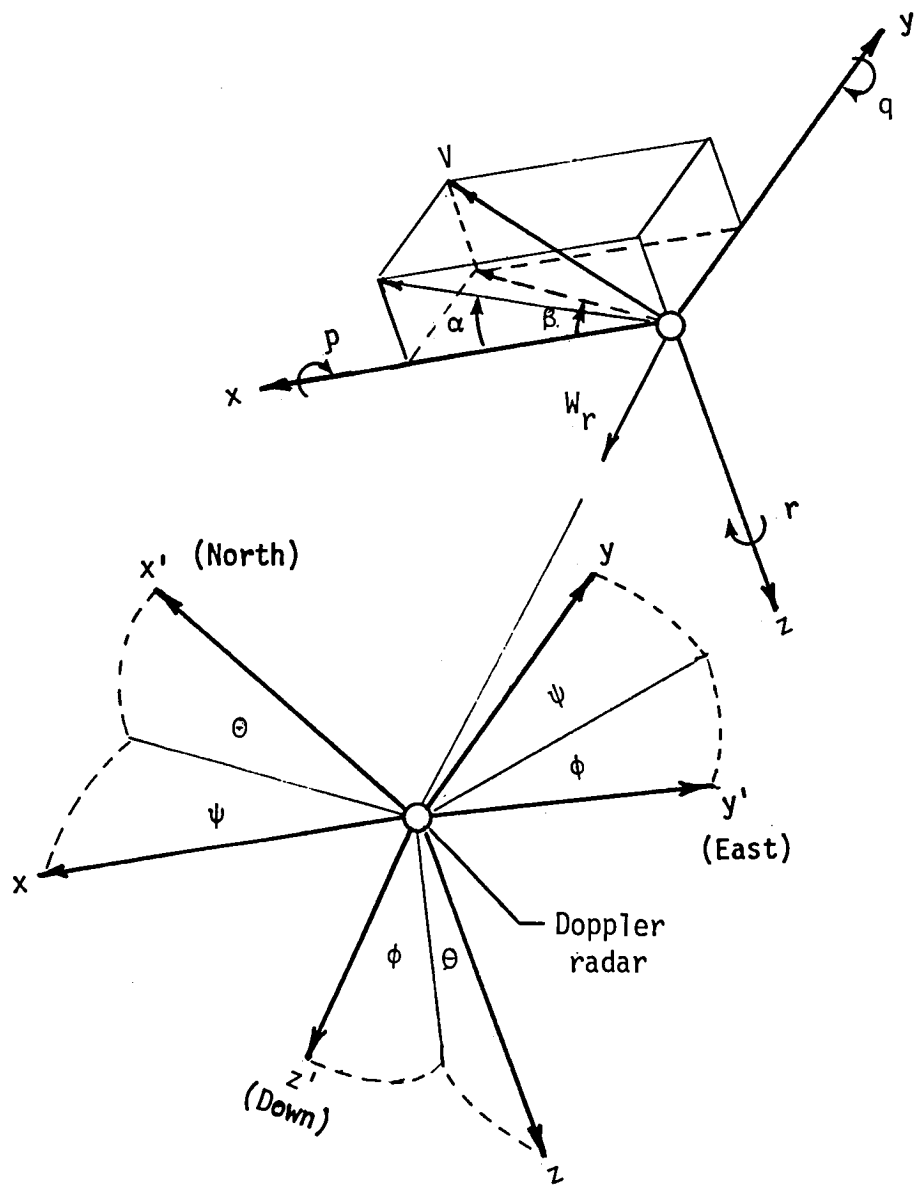

Figure A1. Body axes (x, y, z) relative to an Earth-fixed system (x', y', z') and definition of angle of attack and sideslip. The F-106B body-axis rates p, q, and r are relative to x', y', and z'. The order of rotation from the body to the inertial axis system is ψ, θ, ϕ. The symbol W_r represents the component of the wind velocity, W, in the direction of the Doppler radar.

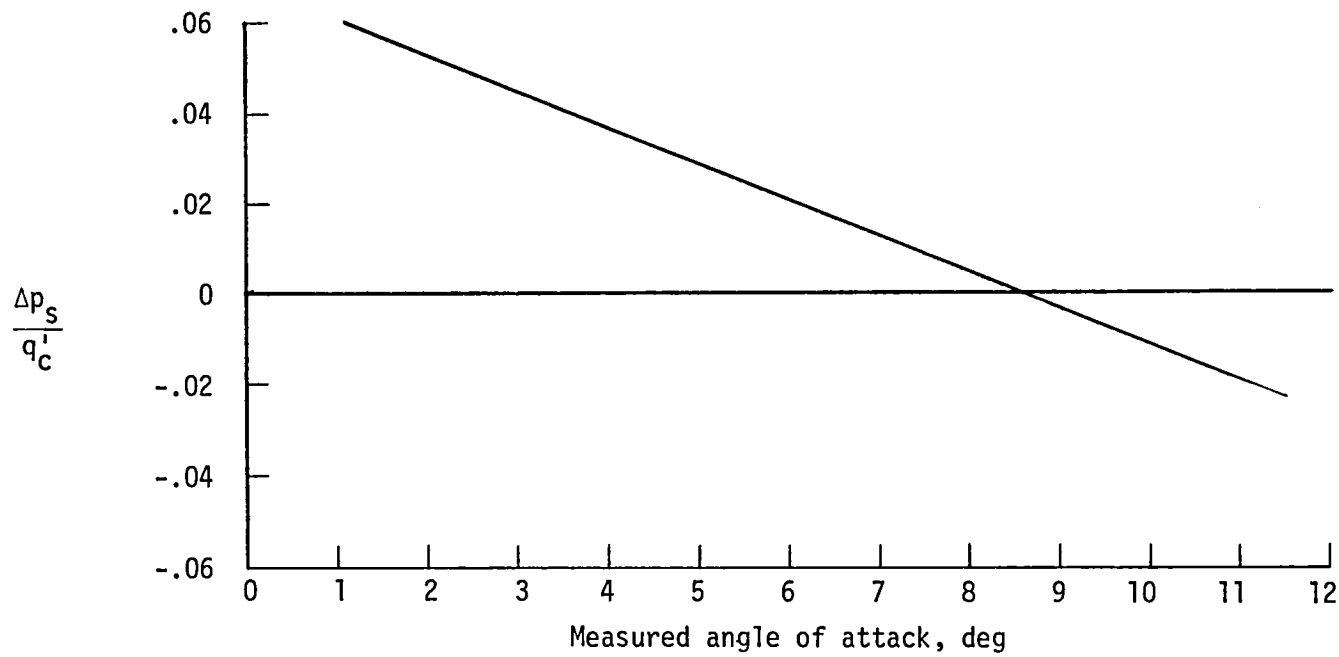

Figure A2. Static-pressure position error calibration.

References

1. Fisher, Bruce D.; and Crabill, Norman L.: Summary of Flight Tests of an Airborne Lightning Locator System and Comparison With Ground-Based Measurements of Precipitation and Turbulence. *1980 Aircraft Safety and Operating Problems,* Joseph W. Stickle, compiler, NASA CP-2170, Part 1, 1981, pp. 251–277.
2. Fisher, Bruce D.; Keyser, Gerald L., Jr.; and Deal, Perry L.: *Lightning Attachment Patterns and Flight Conditions for Storm Hazards '80.* NASA TP-2087, 1982.
3. Deal, Perry L.; Keyser, Gerald L.; Fisher, Bruce D.; and Crabill, Norman L.: Thunderstorm Hazards Flight Research—Program Overview. AIAA-81-2412, Nov. 1981.
4. Lee, J. T.: *Application of Doppler Weather Radar to Turbulence Measurements Which Affect Aircraft.* FAA-RD-77-145, Mar. 1977. (Available from DTIC as AD A048 603.)
5. Lee, J. T.; and Doviak, R. J.: *Field Program Operations—Turbulence and Gust Front Studies.* DOT/FAA/RD-81/108, Nov. 1981. (Available from DTIC as AD A115 447.)
6. Lee, J. T.: *Doppler Radar—Research and Application to Aviation Flight Safety, 1977–1979.* DOT/FAA/RD-81/79, June 1981. (Available from DTIC as AD A109 845.)
7. Rust, W. David; and Doviak, Richard J.: Radar Research on Thunderstorms and Lightning. *Nature,* vol. 297, no. 5866, June 1982, pp. 461–468.
8. Battan, Louis J.: *Radar Observation of the Atmosphere.* Univ. of Chicago Press, c.1973.
9. Doviak, Richard J.; Zrinc', Dusan S.; and Sirmans, Dale S.: Doppler Weather Radar. *Proc. IEEE,* vol. 67, no. 11, Nov. 1979, pp. 1522–1553.
10. Gainer, Thomas G.; and Hoffman, Sherwood: *Summary of Transformation Equations and Equations of Motion Used in Free-Flight and Wind-Tunnel Data Reduction and Analysis.* NASA SP-3070, 1972.
11. Gracey, William: *Measurement of Aircraft Speed and Altitude.* NASA RP-1046, 1980.
12. Richardson, Norman R.: *Dynamic and Static Wind-Tunnel Tests of a Flow-Direction Vane.* NASA TN D-6193, 1971.

1. Report No.	2. Government Accession No.	3. Recipient's Catalog No.
NASA TM-86348		

4. Title and Subtitle	5. Report Date
Comparison of Wind Velocity in Thunderstorms Determined From Measurements by a Ground-Based Doppler Radar and an F-106B Airplane	April 1985
	6. Performing Organization Code: 505-45-13-01
7. Author(s): J. W. Usry, R. Earl Dunham, Jr., and J. T. Lee	8. Performing Organization Report No.: L-15875
9. Performing Organization Name and Address: NASA Langley Research Center, Hampton, VA 23665	10. Work Unit No.
	11. Contract or Grant No.
12. Sponsoring Agency Name and Address: National Aeronautics and Space Administration, Washington, DC 20546	13. Type of Report and Period Covered: Technical Memorandum
	14. Sponsoring Agency Code

15. Supplementary Notes

J. W. Usry and R. Earl Dunham, Jr.: Langley Research Center, Hampton, Virginia.
J. T. Lee: National Severe Storms Laboratory, National Oceanic and Atmospheric Administration, Norman, Oklahoma.

16. Abstract

As a part of the NASA Storm Hazards Program, the wind velocity in several thunderstorms was measured by an F-106B instrumented airplane and a ground-based Doppler radar. This report presents the results of five airplane penetrations of two storms in 1980 and six penetrations of one storm in 1981. Comparisons were made between the radial wind velocity components measured by the radar and the airplane. The correlation coefficients for the 1980 data and part of the 1981 data were 0.88 and 0.78, respectively. It is suggested that larger values for these coefficients may be obtained by improving the experimental technique and in particular by slaving the radar to track the airplane during such tests.

17. Key Words (Suggested by Authors(s))	18. Distribution Statement
Wind velocity Doppler radar Aircraft measurements	Unclassified—Unlimited Subject Category 03

19. Security Classif.(of this report)	20. Security Classif.(of this page)	21. No. of Pages	22. Price
Unclassified	Unclassified	37	A03

For sale by the National Technical Information Service, Springfield, Virginia 22161

NASA-Langley, 1985

National Aeronautics and
Space Administration

Washington, D.C.
20546

Official Business
Penalty for Private Use, $300

THIRD-CLASS BULK RATE

Postage and Fees Paid
National Aeronautics and
Space Administration
NASA-451

NASA

POSTMASTER: If Undeliverable (Section 158
Postal Manual) Do Not Return